AFRL-VA-WP-TR-2002-3089

IMPACT OF PARAMETER VARIATION ON DAMAGE TOLERANCE ANALYSIS ESTIMATES

David H. Wieland
Harry Millwater

Southwest Research Institute
6220 Culebra Road
San Antonio, TX 78228

NOVEMBER 2002

Final Report for 01 October 2000 – 31 May 2002

Approved for public release; distribution is unlimited.

AIR VEHICLES DIRECTORATE
AIR FORCE RESEARCH LABORATORY
AIR FORCE MATERIEL COMMAND
WRIGHT-PATTERSON AIR FORCE BASE, OH 45433-7542

NOTICE

USING GOVERNMENT DRAWINGS, SPECIFICATIONS, OR OTHER DATA INCLUDED IN THIS DOCUMENT FOR ANY PURPOSE OTHER THAN GOVERNMENT PROCUREMENT DOES NOT IN ANY WAY OBLIGATE THE U.S. GOVERNMENT. THE FACT THAT THE GOVERNMENT FORMULATED OR SUPPLIED THE DRAWINGS, SPECIFICATIONS, OR OTHER DATA DOES NOT LICENSE THE HOLDER OR ANY OTHER PERSON OR CORPORATION; OR CONVEY ANY RIGHTS OR PERMISSION TO MANUFACTURE, USE, OR SELL ANY PATENTED INVENTION THAT MAY RELATE TO THEM.

THIS REPORT HAS BEEN REVIEWED BY THE OFFICE OF PUBLIC AFFAIRS (ASC/PA) AND IS RELEASABLE TO THE NATIONAL TECHNICAL INFORMATION SERVECE (NTIS). AT NTIS, IT WILL BE AVAILABLE TO THE GENERAL PUBLIC, INCLUDING FOREIGN NATIONS.

THIS TECHNICAL REPORT HAS BEEN REVIEWED AND IS APPROVED FOR PUBLICATION.

ARVIND NAGAR
Aerospace Engineer
Analytical Structural Mechanics Branch
Structures Division

JAMES W. ROGERS JR., MAJ, USAF
Chief, Analytical Structural Mechanics Branch
Structures Division

JEFFREY S. TURCOTTE, LTC, USAF
Chief
Structures Division

COPIES OF THIS REPORT SHOULD NOT BE RETURNED UNLESS RETURN IS REQUIRED BY SECURITY CONSIDERATIONS, CONTRACTUAL OBLIGATIONS, OR NOTICE ON A SPECIFIC DOCUMENT.

REPORT DOCUMENTATION PAGE

Form Approved
OMB No. 0704-0188

1. REPORT DATE *(DD-MM-YY)*	2. REPORT TYPE	3. DATES COVERED *(From - To)*
November 2002	Final	10/01/2000 – 05/31/2002

4. TITLE AND SUBTITLE
IMPACT OF PARAMETER VARIATION ON DAMAGE TOLERANCE ANALYSIS ESTIMATES

5a. CONTRACT NUMBER
N/A

5b. GRANT NUMBER

5c. PROGRAM ELEMENT NUMBER
N/A

6. AUTHOR(S)
David H. Wieland
Harry Millwater

5d. PROJECT NUMBER
N/A

5e. TASK NUMBER
N/A

5f. WORK UNIT NUMBER
N/A

7. PERFORMING ORGANIZATION NAME(S) AND ADDRESS(ES)
Southwest Research Institute
6220 Culebra Road
San Antonio, TX 78228

8. PERFORMING ORGANIZATION REPORT NUMBER
SWRI 18.04064

9. SPONSORING/MONITORING AGENCY NAME(S) AND ADDRESS(ES)
Air Vehicles Directorate
Air Force Research Laboratory
Air Force Materiel Command
Wright-Patterson Air Force Base, OH 45433-7542

10. SPONSORING/MONITORING AGENCY ACRONYM(S)
AFRL/VA SM

11. SPONSORING/MONITORING AGENCY REPORT NUMBER(S)
AFRL-VA-WP-TR-2002-3089

12. DISTRIBUTION/AVAILABILITY STATEMENT
Approved for public release; distribution is unlimited.

13. SUPPLEMENTARY NOTES
Report contains color. This technical effort was financially supported by the Department of Veterans Affairs V674P-2995, delivery order 674-W00149.

14. ABSTRACT ***(Maximum 200 Words)***
This study was conducted to determine the effects of variations in damage tolerance analysis parameters on fatigue crack growth life. The damage tolerance analysis with variations in input parameters was performed at fatigue critical locations in two different aircraft types using probabilistic sensitivity analysis methods. Up to 12 input parameters. The geometry correction factors, stress spectrum scale factor and stress intensity factor values were found to affect the damage tolerance analysis estimates.

15. SUBJECT TERMS
Damage Tolerance, Crack Growth, Life Analysis, Damage Parameters, Fatigue Critical Locations, Probabilistic Sensitivity Analysis

16. SECURITY CLASSIFICATION OF:			17. LIMITATION OF ABSTRACT:	18. NUMBER OF PAGES	19a. NAME OF RESPONSIBLE PERSON (Monitor)
a. REPORT	b. ABSTRACT	c. THIS PAGE			Arvind Nagar
Unclassified	Unclassified	Unclassified	SAR	60	19b. TELEPHONE NUMBER *(Include Area Code)* (937) 904-6777

Standard Form 298 (Rev. 8-98)
Prescribed by ANSI Std. Z39-18

Table of Contents

List of Figures

List of Tables

Executive Summary

The damage tolerance analysis (DTA) process involves the use of a variety of input parameters to compute fatigue crack growth life. This program used modern probabilistic techniques to investigate how the typical variation on input parameters effects crack growth life. A key objective of this work was to determine the effect of uncertainties in DTA modeling parameters on crack growth life using probabilistic sensitivity analyses. The results of these sensitivity studies may be used to provide further direction for future funding for developing DTA technology by AFRL.

In a traditional (deterministic) engineering analysis, such as the DTAs performed for aircraft structures, input parameters for the models are assumed to be fixed, single-value constants and conservative choices are necessarily made for safety. However, in a probabilistic analysis, input parameters may be considered as random variables and described statistically. For this research, mean values and specific distributions for the input random variables were developed from available test data, tear down results and analysis. Two different aircraft fatigue critical locations were analyzed for three (3) different input stress spectrums along with two different crack growth model idealizations. A total of 12 or 13 random variables were included in the probabilistic sensitivity studies, depending on the fatigue critical location (FCL) analyzed.

While these analyses were performed for two specific fatigue critical locations, the input data is considered to be representative of typical aircraft fatigue critical locations. The results and conclusions are conditioned upon the assumptions made herein. With this caveat in mind, and compared to the other variables considered, it appears the geometry correction factor, hole diameter, stress spectra scale factor, and crack growth rate data are the most critical variables.

The geometry correction factor (beta) is the only parameter that shows crack sensitivity to both the mean value and standard deviation for all the simulations. Including the effects of the countersink correction factor has a large effect on the overall simulation results. This indicates that properly modeling the stress intensity factors is critical for damage tolerance analysis and that oversimplification may be non-conservative.

The results are sensitive to the stress spectrum scale factor mean value, but not the standard deviation. This is an indication of the importance of a good stress analysis that accurately predicts the state of stress at the FCL. It also indicates the importance of the stress levels in a component part for determining the damage tolerance life. The crack growth results are sensitive to the crack growth rate scatter in the higher ΔK range. This indicates that reducing the variation in crack growth rate may help reduce the scatter in damage tolerance test and analysis results.

The results are not sensitive to the fastener spacing or edge distance (ED). This is an indication that relaxing the tolerance on hole placement may be possible as long as a minimum ED or fastener spacing is maintained. Relaxing the tolerance on fastener spacing could potentially speed up production.

The crack growth results are not sensitive to fracture toughness but are sensitive to the crack growth rate. This indicates that in the initial design process when materials are being selected; the crack growth rate may be a more important consideration than fracture toughness.

These analyses were instructive from the point of view of determining the importance of key DTA variables and demonstrating the application of probabilistic methods for crack growth analyses. The current program was limited to investigating a given usage starting with rogue flaw sizes. It is recommended that this method be extended to investigate variation in aircraft usage and the use of a typical manufacturing flaw size or a crack initiation model. Performing probabilistic crack growth analyses for an entire aircraft would help quantify the overall fleet reliability and facilitate development of risk-based inspection intervals. It is also recommended that probabilistic analyses such as those described herein be investigated for application to the design of new aircraft.

List of Abbreviations and Symbols

Organizations:

AFRL	Air Force Research Lab
NASA	National Aeronautics and Space Administration
SwRI	Southwest Research Institute

Terminology:

AFGROW	AFRL/VASM Fatigue Crack Growth Software
CDF	Cumulative Distribution Function
CRACKS98	UDRI Fatigue Crack Growth Software
DTA	Damage Tolerance Analysis
FCL	Fatigue Critical Location
FEA	Finite Element Analysis
FEM	Finite Element Model
NASGRO	NASA Fatigue Crack Growth Analysis Software
NESSUS	SwRI Probabilistic Analysis Software

Damage Tolerance Analysis Symbols:

a	crack depth
a/c	crack aspect ratio
c	half surface crack length
C	paris coefficient
K_{Ic}	plain strain fracture toughness
K_c	plain stress fracture toughness
m	Walker equation constant
n	paris exponent
R	stress ratio

Probabilistic Analysis Symbols:

dP_f/dm_i	change in failure probability due to a change in the mean value of a random variable
dP_f/ds_I	change in failure probability due to a change in the standard deviation of a random variable
μ	mean value
σ	standard deviation
P_f	probability of failure
g	limit state
N	total number of Monte Carlo samples
N_f	number of failure points during Monte Carlo sampling

1.0 INTRODUCTION

1.1 Background

The USAF has been using Damage Tolerance Analysis (DTA) methods since the early seventies to design new aircraft and determine inspection intervals for aging aircraft. New aircraft are designed using DTA such that a rogue flaw in the structure will not grow to failure between inspections. Aircraft that were designed before the widespread use of DTA methods have been reanalyzed using DTA methods to determine inspection intervals in order to ensure safety of flight. Over the years, the accuracy of various portions of the damage tolerance analysis has been improved substantially, and is still being improved, while other areas of the process are not much better than they were thirty years ago. For example, the ability to determine stress intensity factors for nonstandard geometry has improved due to the use of better computational techniques. However, the ability to predict how an aircraft will be used is still based on how the previous aircraft of that type was used.

A much better understanding now exists of the nature and degree of variation the key DTA parameters can exhibit. Also, continued development of probabilistic analysis procedures has progressed such that they can now speedily and economically handle the greatly added complexity of these variables being characterized as distributions rather than a single value. These distributions represent the variations that these parameters can exhibit in realistic structure constructed using the state-of-the-art methods in today's aircraft. The first step in understanding the impact of this analysis improvement is an assessment of the uncertainties/variations in typical DTA inputs, and the impact the uncertainties have on life estimates. From these results, guidance can be gained as to where and how these probabilistic methods should be incorporated into standard DTA efforts.

1.2 Objective

The damage tolerance analysis process involves the use of a variety of input parameters, many of which have associated with them inherent uncertainty (as in material properties) or statistical uncertainty (as in loads, initial crack sizes, geometry, etc.). In addition, the assumptions contained in the analysis methods may result in modeling errors, i.e., the use of simplified models to represent complex behavior. The primary objectives of this work, therefore, were to (1) determine the effect of uncertainties in DTA modeling parameters on crack growth life estimates through the use of probabilistic sensitivity analyses, and (2) develop recommendations to assist in providing further direction for the further development of DTA technology by the USAF. For the analyses that are presented in this report, two different FCLs from different types of aircraft were analyzed to ensure results are not only applicable to a single FCL or aircraft type.

1.3 General Approach

For the fatigue crack growth calculations, the AFGROW fatigue crack growth analysis software was selected. Therefore, the initial step in accomplishing the objectives of this project was to interface AFGROW with NESSUS, SwRI's state-of-the-art probabilistic analysis software. While the built-in AFGROW single corner crack at a hole geometry model was primarily used in this study, the probabilistic analysis approach employed herein is straightforward in nature and could easily be used with the other fracture mechanics analysis models contained in AFGROW.

In order to ensure that the results of this analysis were applicable to more than one FCL or aircraft type, an FCL for a highly maneuverable supersonic aircraft wing was analyzed as well as a pressure loaded transport fuselage FCL. The T-38 was chosen for the highly maneuverable aircraft due to the large amount of available data and its Introduction to Fighter Fundamental (IFF) usage. The IFF usage is very severe, and routinely exceeds 8 g's while the aircraft was designed for a 7.3 g limit load. The C-130 was chosen as a typical pressure loaded transport fuselage.

SwRI and the Ogden Air Logistics Center (OO-ALC) depot ASIP engineer identified five T-38 lower wing skin FCLs for possible use on this program. AFRL selected T-38 FCL A-15. A-15 is a countersunk fastener hole in the lower wing skin at the 15% spar and WS 64.8. See Section 4.0 for a complete description of FCL A-15.

SwRI and the Warner-Robins Air Logistics Center (WR-ALC) depot ASIP engineer identified four C-130 fuselage FCLs for possible use on this program. AFRL selected C-130 fuselage FCL CF-15 for this program. CF-15 is a lower fuselage butt splice fastener hole loaded by pressure cycles. See Section 5.0 for a complete description of CF-15.

In a traditional (deterministic) engineering analysis, such as the DTAs performed to date on T-38[1]* and C-130[2], input parameters for the model(s) are assumed to be single-valued (constant) and conservative. However, in a probabilistic analysis, input parameters may be considered as random variables and are described by statistical distributions characterized by mean, standard deviation, and probability distribution type., e.g., normal, lognormal, Weibull. Therefore, a probabilistic analysis can account for the uncertainty or variability associated with each model input parameter. The BestFit computer software was used to determine the mean values, standard deviation and distribution type of the input parameters for the sensitivity studies. The input distributions for each random variable were developed from actual measurements, where possible.

For this program, two different crack growth retardation models were studied: the generalized Willenborg retardation model, and a closure model. The choice between two different crack growth retardation models does not reflect a statistical variation in input data; rather, it provides insight into the difference in results obtained with retardation models of different types. In order to investigate geometry simplification assumptions, the FCLs were analyzed both with and without countersink correction factors. The

*Numbers in square brackets [ ] refer to references listed in Section 7.0

analysis was performed using the Monte Carlo sampling method (see Section 2.3). For each analysis, 5,000 crack growth runs were performed.

1.4 Organization of Report

Section 2.0 of this report gives a general overview of probabilistic methods. Section 3.0 of this report discusses the development of the random variable distributions. Section 4.0 presents the T-38 sensitivity analysis and results. Section 5.0 discusses the C-130 analysis and results. Finally, Section 6.0 contains the observations, conclusions, and recommendations.

2.0 METHODOLOGY

2.1 Selecting a Probability Distribution and Its Parameters

One of the significant challenges to performing a meaningful probabilistic analysis is to determine the input distributions and parameters for a given random variable. The probability of failure results will be dependent in general on the probability distribution selected and it may be difficult to determine which distribution is the best choice.

Certain physical variables are known to be modeled well by the standard distributional forms. If a distribution can be assumed for a given variable, e.g., the normal distribution to model fracture toughness, then the distribution can be fit to data using the method of moments, e.g., estimate the moments of the distribution from the data. The performance of the more accurate, and complicated, maximum likelihood method is often found to be insignificantly better than method of moments.

There are a number of statistical tests to quantify how well a distribution fits data such as Chi-Square [3,4], Kolmogorov-Smirnov [3,4], and Anderson-Darling, [5], and software to apply these tests.

The BestFit software from Palisade computing was used to determine the most appropriate distribution for a given set of data. BestFit applies the Chi-Square, Kolmogorov-Smirnov, and Anderson-Darling tests to a set of data and compares the results from approximately twenty distribution types, e.g., normal, lognormal, Weibull, logistic, extreme value, etc. The distributions are ranked according to the best fit to the data. The user can then review plots of the higher-ranking distributions and select the most appropriate one.

2.2 Overview of NESSUS

The SwRI NESSUS (Numerical Evaluation of Stochastic Structures Under Stress) probabilistic analysis computer program was used to evaluate the probability of failure and the probabilistic sensitivities. NESSUS is a general-purpose probabilistic analysis code that can be interfaced with failure models. NESSUS was originally developed under funding from the NASA Glenn Research Center[6,7]. Figure 2-1 shows a summary of the capabilities of NESSUS.

NESSUS contains a number of probabilistic algorithms that can be used to evaluate the probability of failure such as Monte Carlo sampling, First/Second Order Method, and Advance Mean Value method. First/Second Order Method, and Advance Mean Value method are very fast techniques if a converged solution can be found. This is often but not always the case. Monte Carlo sampling, on the other hand, is slower computationally but more robust and is guaranteed to yield an accurate solution if sufficient samples are used. We used the Monte Carlo sampling method in this research since the solution time is not prohibitive for the examples studied here.

NESSUS
Probabilistic Analysis Software

Inputs
- Graphical user interface
- Free format keyword interface
- Ten probability density functions
- Correlated random variables
- Users/Theory/Examples manual

Outputs
- Cumulative distribution function
- Prob. of failure given performance
- Performance given prob. of failure
- Probabilistic sensitivities with respect to mean and standard deviation
- Confidence bounds
- Empirical cdf and histogram

Analysis Methods
- First-order reliability method
- Second-order reliability method
- Fast probability integration
- Mean-value and advanced mean value
- Response surface method
- Automatic Monte carlo simulation
- Sphere-based importance sampling
- Latin hypercube simulation
- Adaptive importance sampling
- Probabilistic fault-tree
- PFEM Simulation (MCS & LHS)

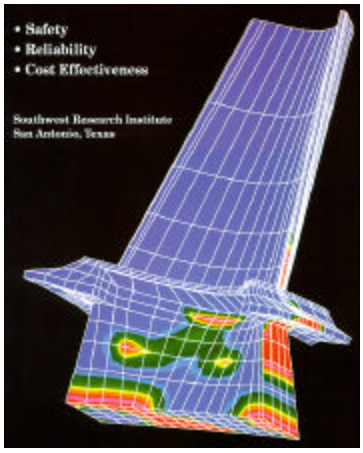

Probability of Exceeding 80ksi

Probabilistic Analysis
- Component reliability
- System reliability
- Risk-based cost analysis
- Automated restart
- Batch processing

Performance Functions
- Analytical (Fortran)
- Analytical (Input deck)
- Numerical (FEM, BEM, other)
- Failure models (Fortran)
- Any combination of the above

NESSUS/FEM module
- Static
- Dynamics
- Nonlinear material
- 1, 2, 3D elements
- Perturbation algorithm

Interfaces
- *NESSUS/FEM*
- *ABAQUS*
- *NASTRAN*
- *PRONTO*
- *User-defined*

Hardware
- Personal computers
- Unix workstations
- Mainframes, supercomputers
- Y2K Compliant

Further Information

210/522-6566
nessus@swri.org
www.swri.org/nessus

Figure 2-1 Summary of NESSUS Capabilities

2.3 Monte Carlo Sampling

2.3.1 Overview

Monte Carlo sampling is a method of statistical trials. The procedure is to generate realizations of random variable inputs (e.g., loads, material properties, and geometries), based on their probability distributions, evaluate the model, and record the results (e.g., fail or no fail). This procedure is repeated many times with new randomly generated inputs. When a sufficient number of samples have been carried out, estimates of the probability of failure and the moments (e.g., mean and standard deviation) of the response may be computed (see Figure 2-2).

Monte Carlo sampling can also be used to compute the probabilistic sensitivities,

$$\frac{\partial P_f}{\partial m_i}, \quad \frac{\partial P_f}{\partial s_i}$$

where P_f is the probability of failure, μ_i and σ_i are the mean and standard deviation of random variable *i*, respectively. These sensitivities indicate the amount of change that would occur in the probability of failure if the mean or standard deviation of a random variable is changed. The sensitivities can be used to determine the relative importance of the random variables.

Monte Carlo is a powerful technique that is very robust and straightforward to use. It is guaranteed to converge to the correct probability solution in the limit as the number of samples, i.e., statistical trials, increases to infinity. The potential drawback is related to computational time in that many realizations, and, thus, much computational time may be required to obtain accurate probability of failure estimates for the low probabilities often found in structural life assessment.

Monte Carlo sampling has extremely broad applicability. It is used in the context of probabilistic analysis in many fields such as engineering (structural), physics, materials science, biology, biomechanics, finance, and games, among others. It is also useful in a non-probabilistic context for evaluating high-dimensional integrals.

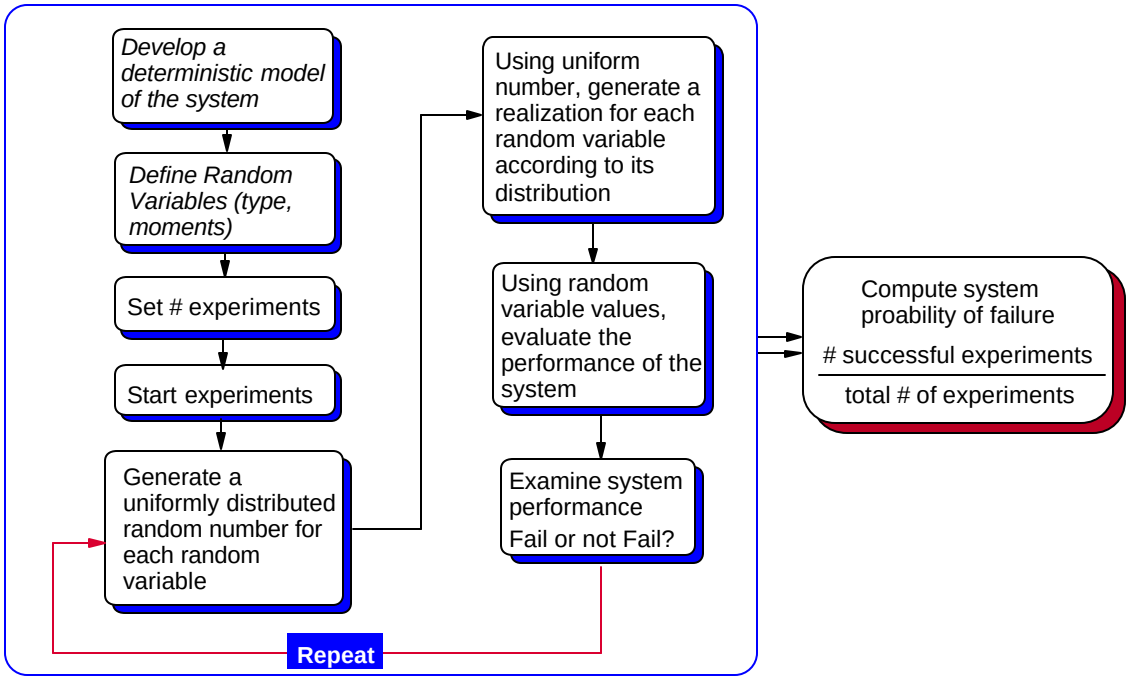

Figure 2-2 Overview of Monte Carlo Method

2.3.2 Failure Model (or Limit State)

The failure model, or limit state, is a statement of the physics of the problem of interest and defines the criteria for failure. In effect, the limit state divides the domain into 'safe'

and 'failure' regions. The probability of failure is the amount of probability located in the failure region.

The limit state for probabilistic computations is formulated such that when evaluated mathematically, a value less than or equal to zero defines failure and a value greater than zero defines safety. The limit state is typically given the symbol *"g"* and formulated such that

$g \leq 0$ - *failure*

$g > 0$ - *safe*

The limit state depends on the analysis being considered and is purely a deterministic equation. Table 2-1 lists some common definitions of failure that could be formulated in a limit state.

Table 2-1 Some Common Limit State Definitions of Failure

cycles-to-failure ≤ cycles of interest
clearance ≤ maximum displacement
fracture toughness ≤ stress intensity factor
J material ≤ J integral
critical crack size ≤ growing crack size
material thickness ≤ corrosion depth
yield strength ≤ stress
creep strength ≤ Larson-Miller parameter

There is no unique definition required of the limit state. Equivalent representations such that $g \leq 0$ defines failure and $g > 0$ defines safety are sufficient. For example, if the limit state is such that the failure occurs when the stress (S) exceeds the material strength (R), the limit state may be represented equivalently in the following forms:

$$g = R - S$$

$$g = R/S - 1$$

$$g = \ln(R/S)$$

In this research, the limit state is defined as $g = N_f - N_o$ where N_f = cycles-to-failure and N_o is a specified number of cycles. The actual cycles-to-failure was determined by AFGROW.

2.3.3 Generating Random Variables

Monte Carlo sampling requires repeated generation of random variable values based on their probability distributions. The generation of random variable values is typically done using the "inverse function method" if the RVs are independent. More sophisticated methods are required if the RVs are correlated. In this research, all random variables are modeled as independent.

Values for independent RVs are generated as follows:

– Generate a uniform random number between zero and one; this value becomes the probability of the random variable.

– Using this probability, invert the cdf to obtain the random variable value that corresponds to this probability.

This procedure is shown mathematically in Figure 2-3.

$$U^* = U[0,1]$$
$$F(x^*) = U^*$$
$$x^* = F^{-1}(U^*)$$

Figure 2-3 Mathematics of Inverse Function Method

Where $U[0,1]$ indicates a uniform distribution with limits zero and one, U^* is a random number between zero and one generated from the uniform distribution, F denotes the random variable cdf, and x^* is the generated realization of random variable X.

The procedure is shown schematically in Figure 2-4.

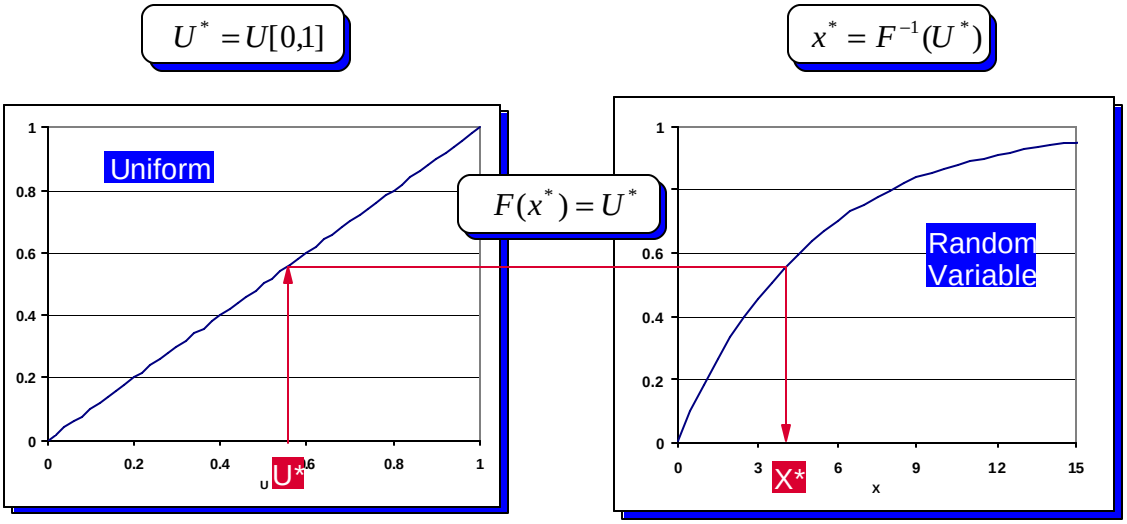

Figure 2-4 Schematic of Inverse Function Method

Figure 2-5 presents an example of generating realizations for an exponential distribution. The values for *U** are merely illustrative. In general, *U** values should be generated randomly.

- Example: exponential distribution with $\lambda = 0.1$ (mean = 10)

$$F(x) = 1 - e^{-lx}$$

$$x^* = F^{-1}(U^*) = -\frac{1}{l}\ln(1-U^*)$$

U*	X*
0.1	1.053
0.3	3.567
0.5	6.931
0.7	12.040
0.9	23.026

Figure 2-5 Example: Generating Random Variable Values

2.3.4 Probability Estimates

In probabilistic life assessment, we are typically interested in determining the probability of failure, i.e., $P[g \le 0]$. The probability of $g \pounds 0$ is estimated by the ratio of the number of failure points divided by the total number of samples as

$$P_f = \frac{N_f}{N}$$

where N is the total number of samples, N_f is the number of samples for which g ≤ 0, and P_f is the estimate of the probability of failure. It is important to realize that P_f is merely an estimate of the true probability of failure that remains forever unknown. Thus, P_f is a random variable and will change if we rerun the simulation, say with a new seed. The variation in P_f, i.e., its standard deviation, is an indication of the accuracy of the answer and can be determined from the binomial distribution as

$$s(P_f) = \sqrt{\frac{(1-P_f)P_f}{N}}$$

Note that the standard deviation of the probability of failure reduces as the square root of the number of samples. Thus, for example, if we want the standard deviation reduced by a factor of two, four times as many samples are required.

2.3.5 Accuracy

2.3.5.1 Error and Confidence Estimation

A natural question arises in Monte Carlo sampling of how many samples to use. The accuracy of the probability estimate will be dependent on the number of samples. We previously showed that the probability of failure estimate from Monte Carlo sampling is itself a random variable and that the standard deviation of the probability of failure varies as the square root of the number of samples.

The confidence bounds of the P_f can be estimated by assuming that the probability of failure is normally distributed (a good approximation). For example, Shooman (1968) developed an equation that can be used to estimate the percent error in a probability estimate as

$$g = 200\sqrt{\frac{1-P_f}{NP_f}}$$

where P_f is the estimated probability of failure, N is the total number of samples, and γ is the estimated percentage error in the computed probability of failure from the true probability of failure. This equation states that we are 95% confident that the percent error in the computed probability of failure, relative to the true probability of failure, is less than γ. For example: given P_f = 0.001, N = 100,000. Then the equation yields a percent error of 20%. Thus, we are 95% certain that the true probability of failure lies

within 0.001 ± 20% or P_f lies within the range [8E-4, 1.2E-3] with an expected value of 0.001.

We can use this formula to estimate the required number of samples to achieve a desired % error as

$$N = \left(\frac{1 - P_f}{P_f} \right) \left(\frac{200}{g} \right)^2$$

Note that since P_f is usually small for structural reliability analysis, the term 1- P_f can usually be approximated as 1.

A simple but crude rule of thumb is to ensure that you have at least 10 failure points (gives an error of 63% with 95% confidence). The minimum number of sample points to achieve this is

$$N = \frac{10}{P_f} \qquad (P_f < 0.5)$$

$$N = \frac{10}{1 - P_f} \qquad (P_f > 0.5)$$

2.3.6 Sampling-Based Sensitivities

The derivatives $\frac{\partial P_f}{\partial m_i}$, $\frac{\partial P_f}{\partial s_i}$ can be obtained from Monte Carlo sampling as a byproduct of the analysis, i.e., no extra analyses are required[8].

The probability of failure is determined by solving the multidimensional integral

$$P_f = \int_{\Omega} f_{\underset{\sim}{X}}(\underset{\sim}{x}) d\underset{\sim}{x} \tag{1}$$

where $\underset{\sim}{x}$ indicates a vector of random variables, $f_{\underset{\sim}{X}}$ is the joint probability density function of the random variables, and Ω denotes the failure region, i.e., the region of the random variable space where $g \le 0$. In two dimensions, this integral is the volume of probability in the failure region.

Equation 1 may be written in terms of an "indicator" function, $I(\underset{\sim}{x})$. $I(\underset{\sim}{x})$ is defined such that

$I = 1$ for $g \le 0$ - *failure*

$I = 0$ for $g > 0$ - *safe*

Equation 1 becomes

$$P_f = \int_{\Omega} f_{\underset{\sim}{X}}(\underset{\sim}{x}) d\underset{\sim}{x} = \int_{-\infty}^{\infty} I(\underset{\sim}{x}) f_{\underset{\sim}{X}}(\underset{\sim}{x}) d\underset{\sim}{x} = E[I(\underset{\sim}{x})] \tag{2}$$

where E denotes the expectation operator.

Sensitivities of the probability of failure with respect to the mean and standard deviation of the random variables may be obtained by taking the derivative of equation 2 as

$$\frac{\partial P_f}{\partial q_i} = \int_{-\infty}^{\infty} I(\underset{\sim}{x}) \frac{\partial f_{\underset{\sim}{X}}(\underset{\sim}{x})}{\partial q_i} d\underset{\sim}{x} = \int_{-\infty}^{\infty} \left(I(\underset{\sim}{x}) \frac{\partial f_{\underset{\sim}{X}}(\underset{\sim}{x})}{\partial q_i} \frac{1}{f_X(x_i)} \right) f(x_i) d\underset{\sim}{x}$$

$$= \int_{-\infty}^{\infty} \left(I(\underset{\sim}{x}) \frac{\partial f_X(x_i)}{\partial q_i} \frac{1}{f_X(x_i)} \right) f_{\underset{\sim}{X}}(\underset{\sim}{x}) d\underset{\sim}{x} = E\left[I(\underset{\sim}{x}) \frac{\partial f_X(x_i)}{\partial q_i} \frac{1}{f_X(x_i)} \right] = E[y] \tag{3}$$

Equation 3 indicates that the sensitivity $\frac{\partial P_f}{\partial q_i}$ can be obtained by taking the expected value of the quantity $y = I(\underset{\sim}{x}) \frac{\partial f_X(x_i)}{\partial q_i} \frac{1}{f_X(x_i)}$. This can be accomplished using the same samples that were used to estimate P_f as

$$E[y] = \frac{1}{N} \sum_{j=1}^{N} y_j \tag{4}$$

where N is the number of samples and ψ_j denotes the value of ψ for a particular realization of random variables. Thus, no additional computations are required and the sensitivities can be obtained from standard Monte Carlo sampling.

2.3.6.1 Example

The problem of estimating the probability of failure given a strength (or capacity), denoted "R," and a stress (or load), denoted "S," occurs frequently (shown schematically in Figure 2-6). As long as the probability distributions of R and S are known (or can be estimated), this problem is one of two random variables and the probability of failure may be determined in a straightforward and efficient manner.

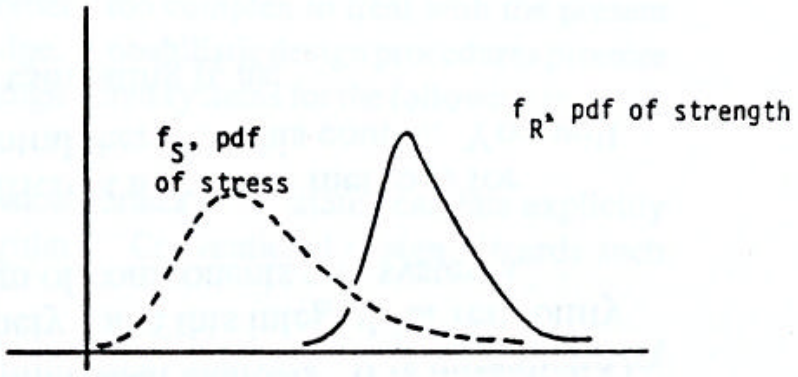

Figure 2-6 Strength-Stress Diagram

The limit state is

$$g = R - S$$

and the probability of failure can be determined by solving the two-dimensional integral

$$P_f = \int_0^{\infty} \int_0^{s} f_S(s) f_R(r) dr ds \tag{5}$$

with integration domain shown in Figure 2-7, and f_S and f_R are the pdfs of the stress and strength, respectively.

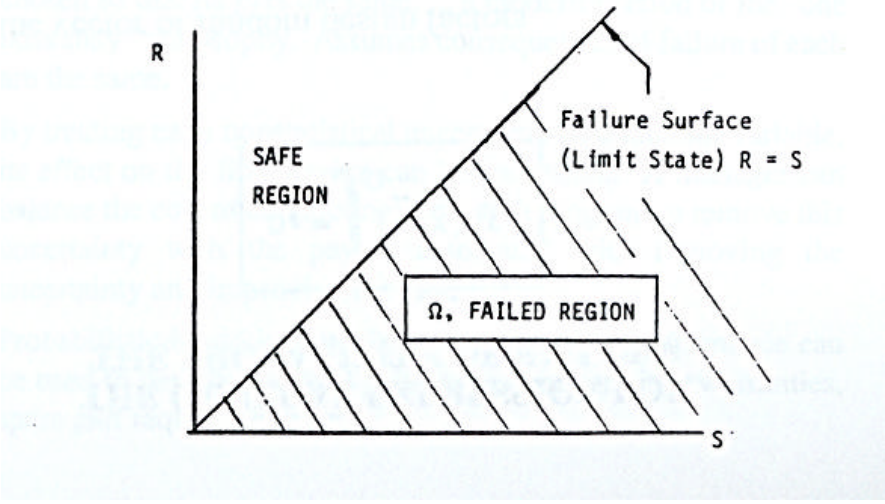

Figure 2-7 Strength-Stress Integration Domain

This integral may be reduced to a one-dimensional integral and is straightforward to compute numerically as

$$P_f = \int_0^\infty f_S(s) F_R(s) ds \tag{6}$$

where F_R is the cdf of the strength.

The sensitivities $\frac{\partial P_f}{\partial m_i}$, and $\frac{\partial P_f}{\partial s_i}$ can be obtained by perturbing the mean and standard deviation of each random variable and recomputing the probability of failure. The sensitivity is determined in the limit as μ or σ approaches zero.

$$\frac{\partial P_f}{\partial m_i} = \lim_{m \to 0} \frac{P_f[m_i + \Delta m_i, s]}{\Delta m_i} \tag{7}$$

and

$$\frac{\partial P_f}{\partial s_i} = \lim_{s \to 0} \frac{P_f[m, s_i + \Delta s_i]}{\Delta s_i}. \tag{8}$$

Consider the following example. The strength is a normal random variable with the mean equal to 80 ksi and the standard deviation equal to 4 ksi. The stress is an extreme value distribution with mean equal to 55 ksi and standard deviation equal to 8 ksi. The probability of failure is computed from equation 6 as P_f = 0.012401. If the mean of the stress is changed to 57 ksi, the distribution shifts to the right and the probability of failure increases as shown in Figure 2-8. The probability of failure equals 0.0170303 and $\frac{\Delta P_f}{\Delta m_S} = \frac{.012401 - .017003}{55 - 57} = 0.002314$. As the change in μ_s is made smaller and smaller, the ratio $\frac{\Delta P_f}{\Delta m_S}$ approaches 0.00197035.

Similarly, the mean value of the strength can be perturbed, see Figure 2-8b and the probability of failure evaluated. As the perturbation becomes small $\frac{\Delta P_f}{\Delta m_R}$ approaches -0.00196866.

The standard deviation of the stress and strength can be perturbed similarly, see Figures 2-8c and 2-8d, to yield $\frac{\partial P_f}{\partial s_S}$ = 0.00554251 and $\frac{\partial P_f}{\partial s_R}$ = 0.00124231. Note, $\frac{\partial P_f}{\partial m_i}$, and $\frac{\partial P_f}{\partial s_i}$ have units of ksi^{-1}. We see that the probability of failure increases when we

increase the standard deviation of either the stress or the strength (other factors being constant). These results are summarized in Table 2-1.

Solving this problem using the Monte Carlo sampling method within NESSUS yields P_f = 0.012401. The sensitivity results, shown in Table 2-2, are obtained from a single analysis and do not require multiple solutions. As a result, this method is much more efficient than perturbing the mean or standard deviation and rerunning the analysis. The results from NESSUS are shown in Table 2-3. These results agree closely with that obtained from equations 7 and 8.

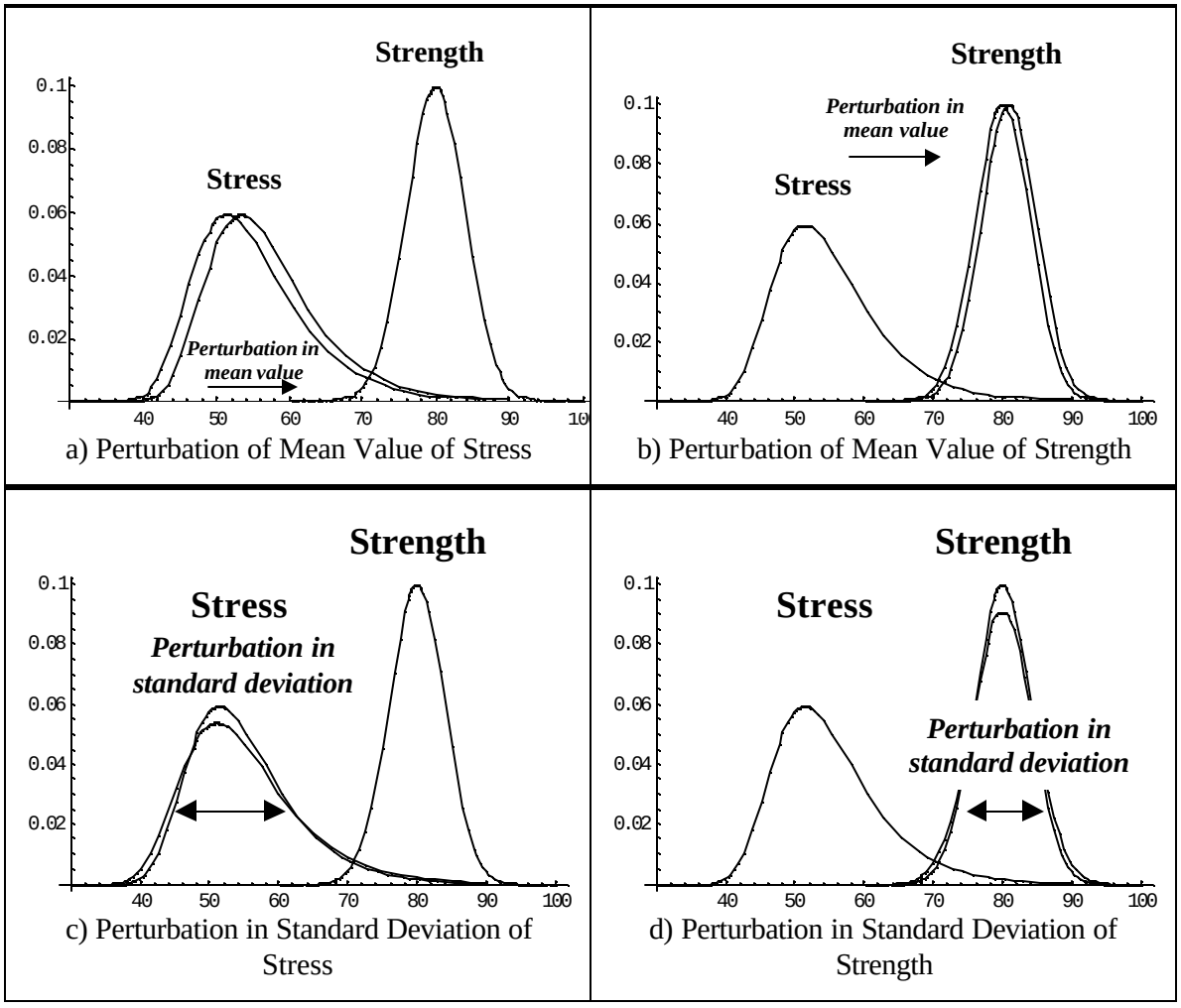

a) Perturbation of Mean Value of Stress

b) Perturbation of Mean Value of Strength

c) Perturbation in Standard Deviation of Stress

d) Perturbation in Standard Deviation of Strength

Figure 2-8 Examples of Perturbation of the Mean and Standard Deviation

Table 2-2 Sensitivity Results Using Equation 7 and 8

$\frac{\partial P_f}{\partial m_S} = 0.001970$	$\frac{\partial P_f}{\partial m_R} = -0.001969$
$\frac{\partial P_f}{\partial s_S} = 0.005542$	$\frac{\partial P_f}{\partial s_R} = 0.001242$

Table 2-3 Sensitivity results using NESSUS

$\frac{\partial P_f}{\partial m_S} = 0.001976$	$\frac{\partial P_f}{\partial m_R} = -0.001925$
$\frac{\partial P_f}{\partial s_S} = 0.006479$	$\frac{\partial P_f}{\partial s_R} = 0.001161$

3.0 RANDOM VARIABLE DEVELOPMENT

For this project, the goal was to use real-world data to generate the random variable distributions to the maximum extent possible. There were either 12 or 13 random variables used in the analysis depending on which FCL was being analyzed. Some of the random variables were common to both the T-38 and C-130. Others were unique to the given FCL. The measured data was fit with the BestFit software program. BestFit does a number of calculations on the data to determine which equation fits the data best. BestFit was limited so that it only used equations that are compatible with the NESSUS probabilistic code.

3.1 Common Random Variables

The random variables common to the T-38 and C-130 FCL are rogue flaw size, crack aspect ratio, stress intensity geometry factor (beta), yield strength, plain strain fracture toughness, plain stress fracture toughness, and crack growth rate. The crack growth rate is modeled as three different random variables.

The rogue flaw size distribution was determined using T-38 wing tear down data from the –29 wing fatigue test [9]. At the end of the test, cracks from 23 wing fastener holes were grown back wards to determine the equivalent initial flaw size [10]. Since rogue flaws are inherently rare, no other data is available to determine their distribution. For this project we fit the initial flaw size distribution with a Weibull equation, then offset it 0.0446369 inches, so that the mean of the distribution was 0.050-inch, which is the rogue flaw size used in DTA. Figure 3-1 shows a graph comparing the input data to the BestFit Weibull equation. Since there are no teardown results available for the C-130, it was assumed the T-38 data was applicable to the C-130.

At the top of the BestFit plots are the distribution equation type (Weibull,, extreme value, etc.), and the BestFit equation variables such as α and β for the Weibull equation, or a and b for the extreme value equation. It should be noted that these variables are not used in NESSUS. NESSUS requires the input of the mean, standard deviation and equation type, instead.

The flaw aspect ratio distribution was determined from the same full-scale wing test result referenced above. An extreme value distribution was chosen. Figure 3-2 shows the comparison of the measured data to the extreme value distribution.

The variation in the geometry correction factor, beta, was evaluated using three different geometry correction factor equations at 23 different crack lengths. Geometry correction factors were determined for a corner crack at a fastener hole in a wide plate using the AFGROW software, the Cracks98 Software, and the NASGRO software. The results for 23 different crack lengths were then normalized by the AFGROW results, since AFGROW was the computer code used in this project. A distribution was then fit to the normalized results. Figure 3-3 show the comparison between the normalized beta factors and the extreme value distribution.

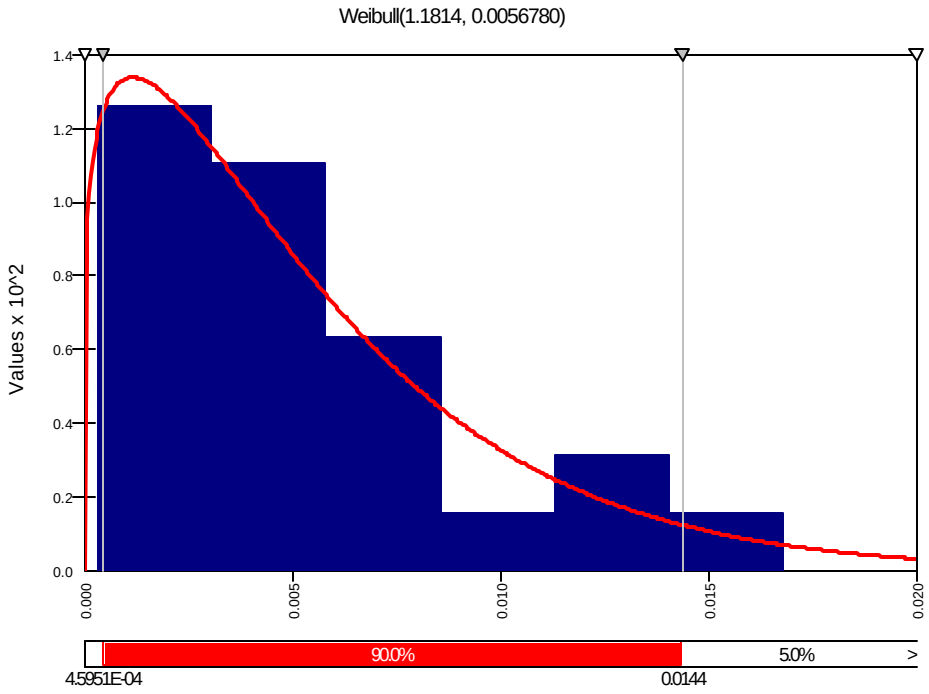

Figure 3-1 EIFS Density Distribution

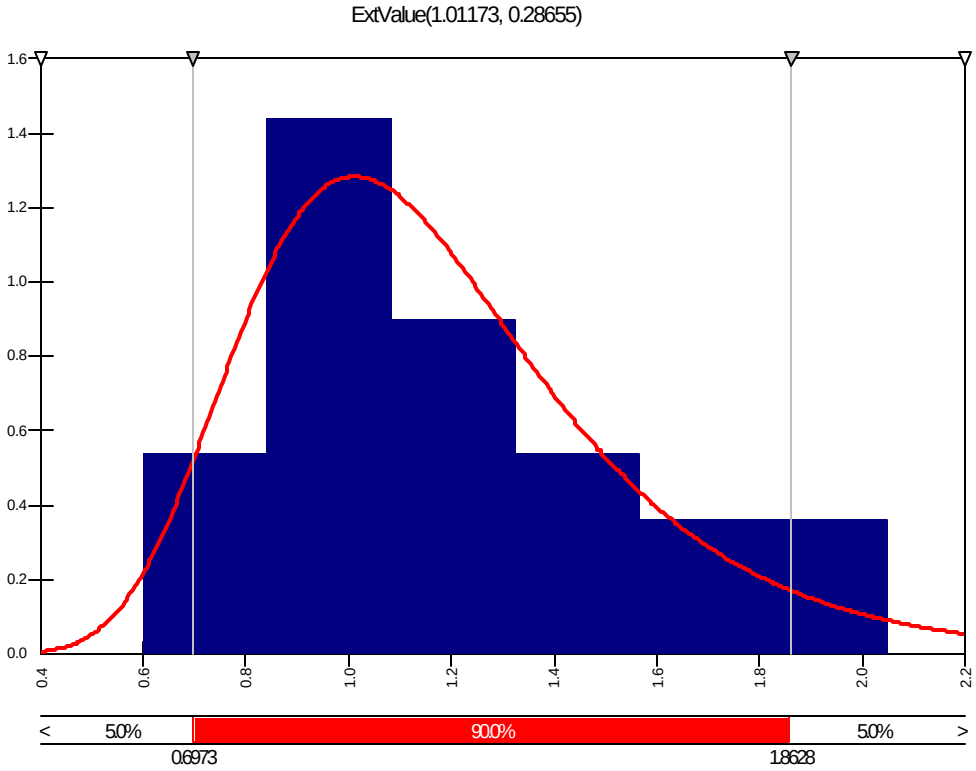

Figure 3-2 Aspect Ratio Density Distribution

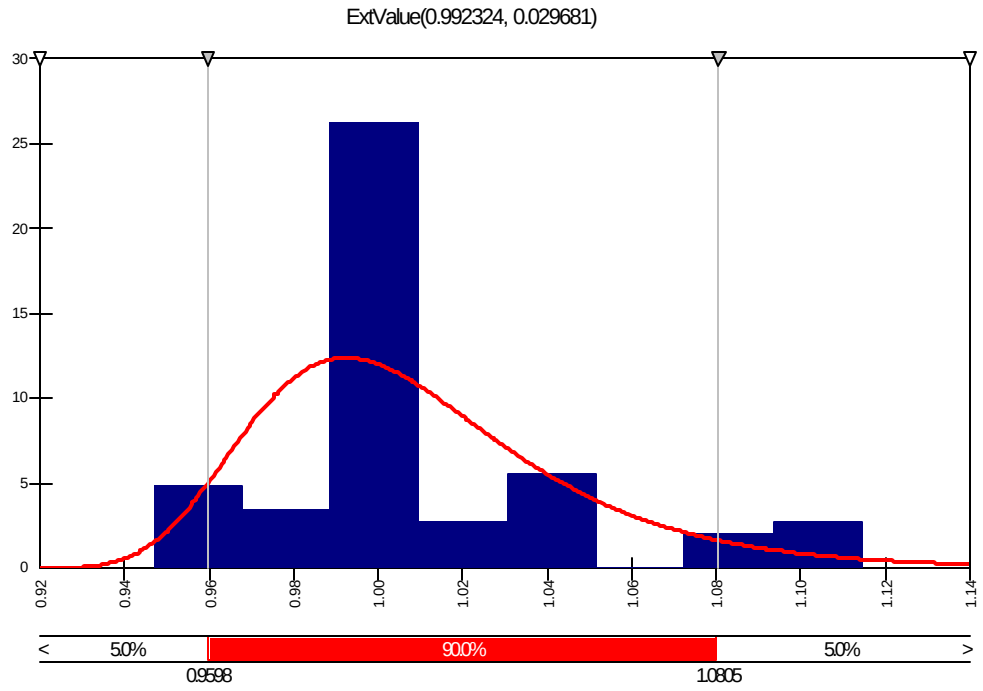

Figure 3-3 Beta Density Distribution

The material data was developed from various test performed by SwRI on 7075-T735 aluminum over the past 20 years [11, 12, 13, and 14]. The yield strength distribution is based on 15 tests. Figure 3-4 shows a comparison of the input data to the BestFit normal distribution. As can be seen in this figure one set of test data was below the B bases allowable for 7075-T735, skewing the distribution slightly.

The fracture toughness distribution was developed from the above references for 11 valid fracture toughness tests. Figure 3-5 shows a comparison of the test data density distribution to the normal fit. As can be seen in this figure the test results are in two different groups indicating additional data would be useful.

SwRI did not have test data for plain stress fracture toughness for the thickness of interest. In order to develop data, the equations in the NASGRO manual for estimating the plain stress fracture toughness as a function of the material yield strength and plain strain fracture toughness was used. Figure 3-6 shows a comparison of the estimated plain stress fracture toughness data density distribution to a normal fit. Again, since the plain stress data is based on the plain strain data, two distinct groups of data appear.

The crack growth rate data used the results of the previously mentioned material tests. Figure 3-7 shows the da/dN verses ΔK test data for 199 test points at various R ratios. A segmented Walker equation was chosen for use on this project of the form:

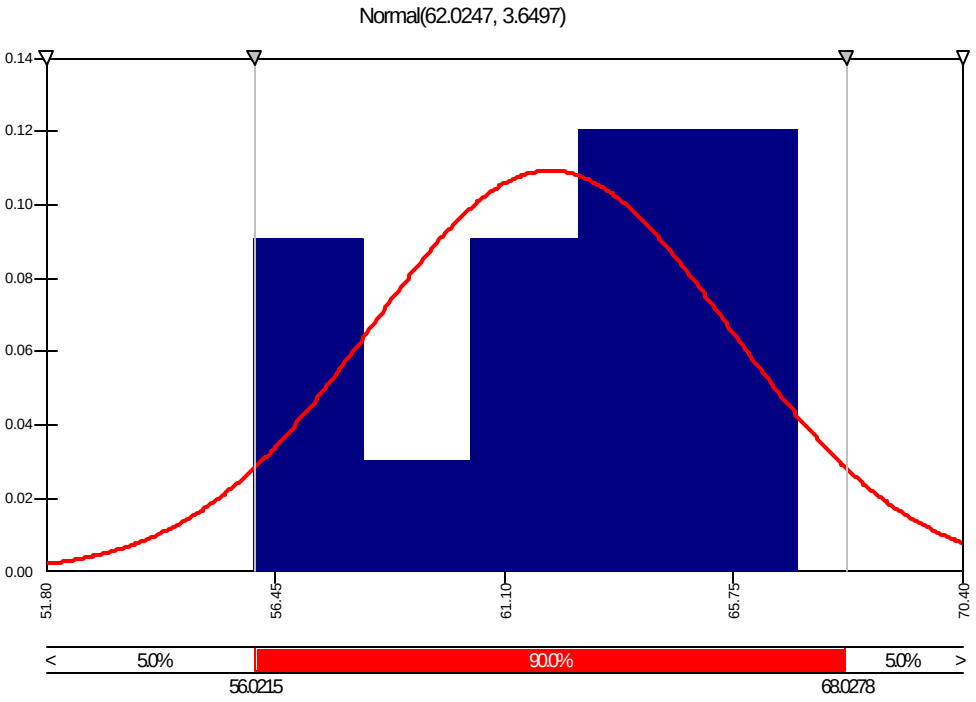

Figure 3-4 Yield Strength Density Distribution

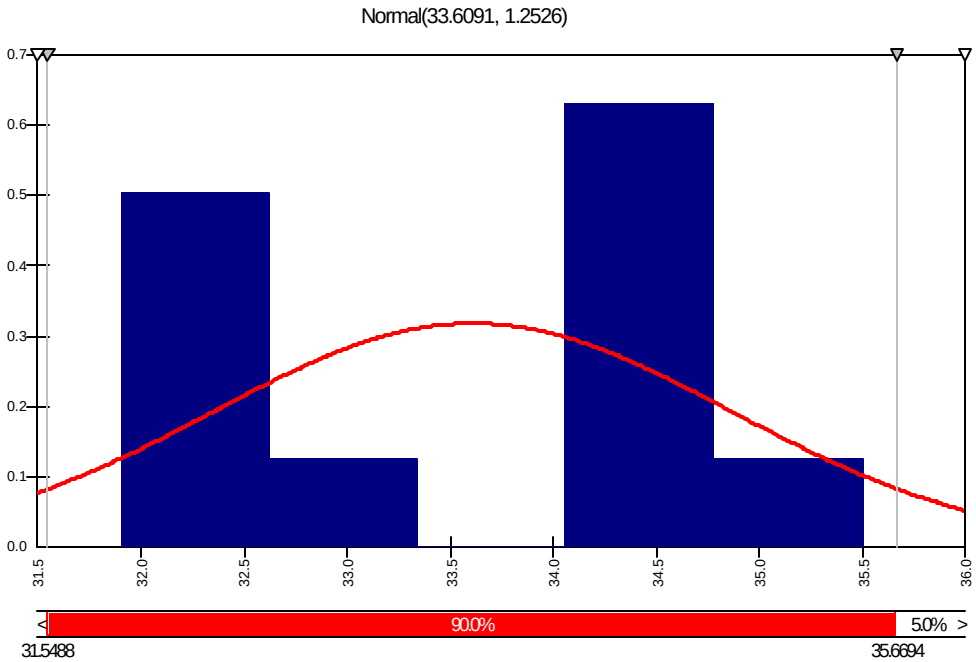

Figure 3-5 Plain Strain Fracture Toughness Density Distribution

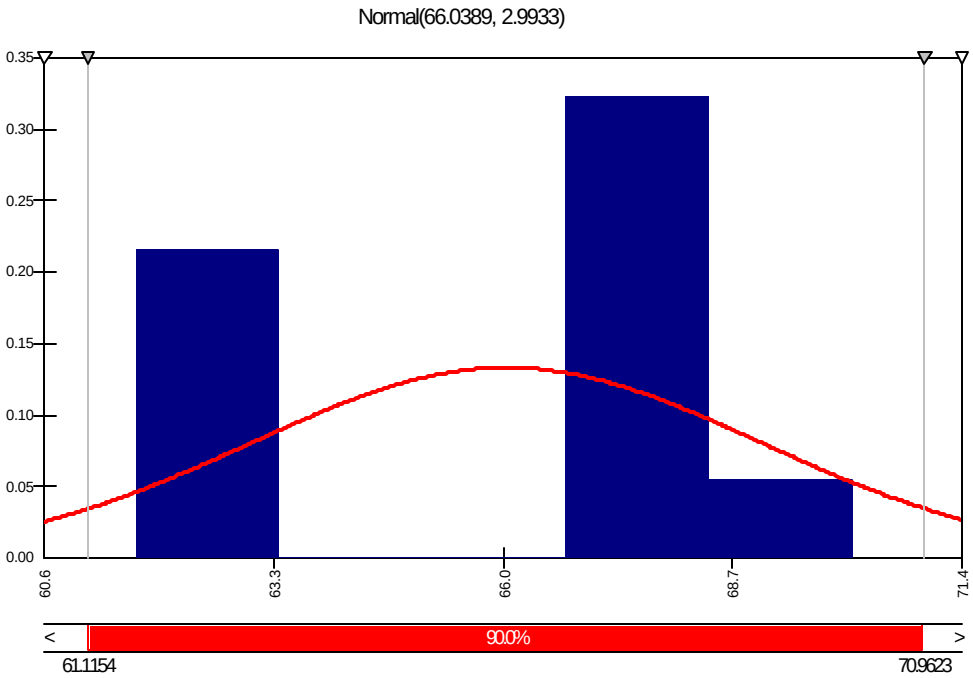

Figure 3-6 Plain Stress Fracture Toughness Density Distribution

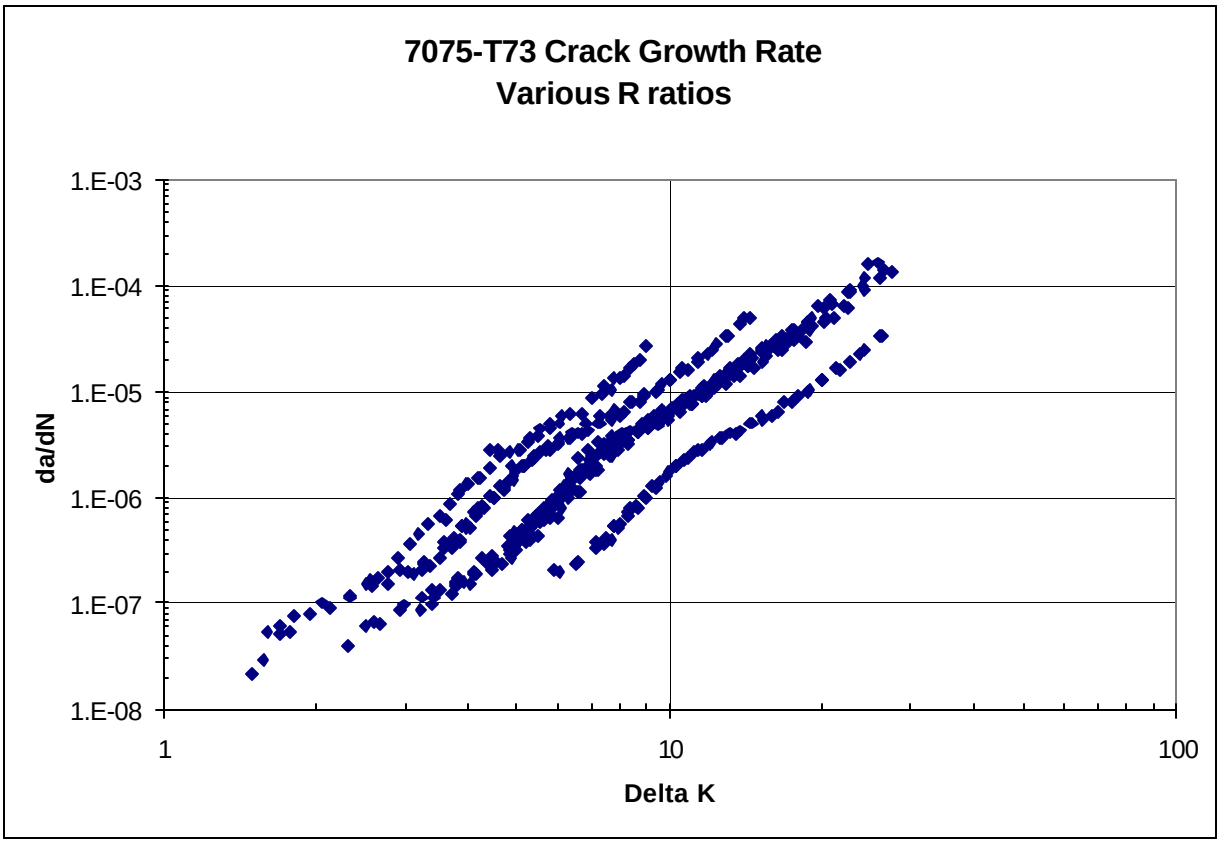

Figure 3-7 Crack Growth Rate Data for 7075-T73

$$da/dN=C[\ \Delta K(1-R)^{(m-1)}]^n$$

where C, m, and n are empirically derived material constants. The purpose of the Walker equation is to collapse the da/dN data for different R ratios down to a single curve. By using an m value of 0.57 and an R ratio cut off value of 0.67, Figure 3-8 shows that the da/dN data collapses well. Since there is a kink in the collapsed data a three-segmented walker equation was used to account for the kink. The exponent "n" is equal to 2.5, 4.6, or 3.15 for the first, second and third segments respectively. Knowing m, n, and R, C is solved for each test point, in order to develop the da/dN distributions. This resulted in distributions for each segment of the Walker equation, C1, C2, and C3. Figures 3-9 thru 3-11 show the density distribution for each segment.

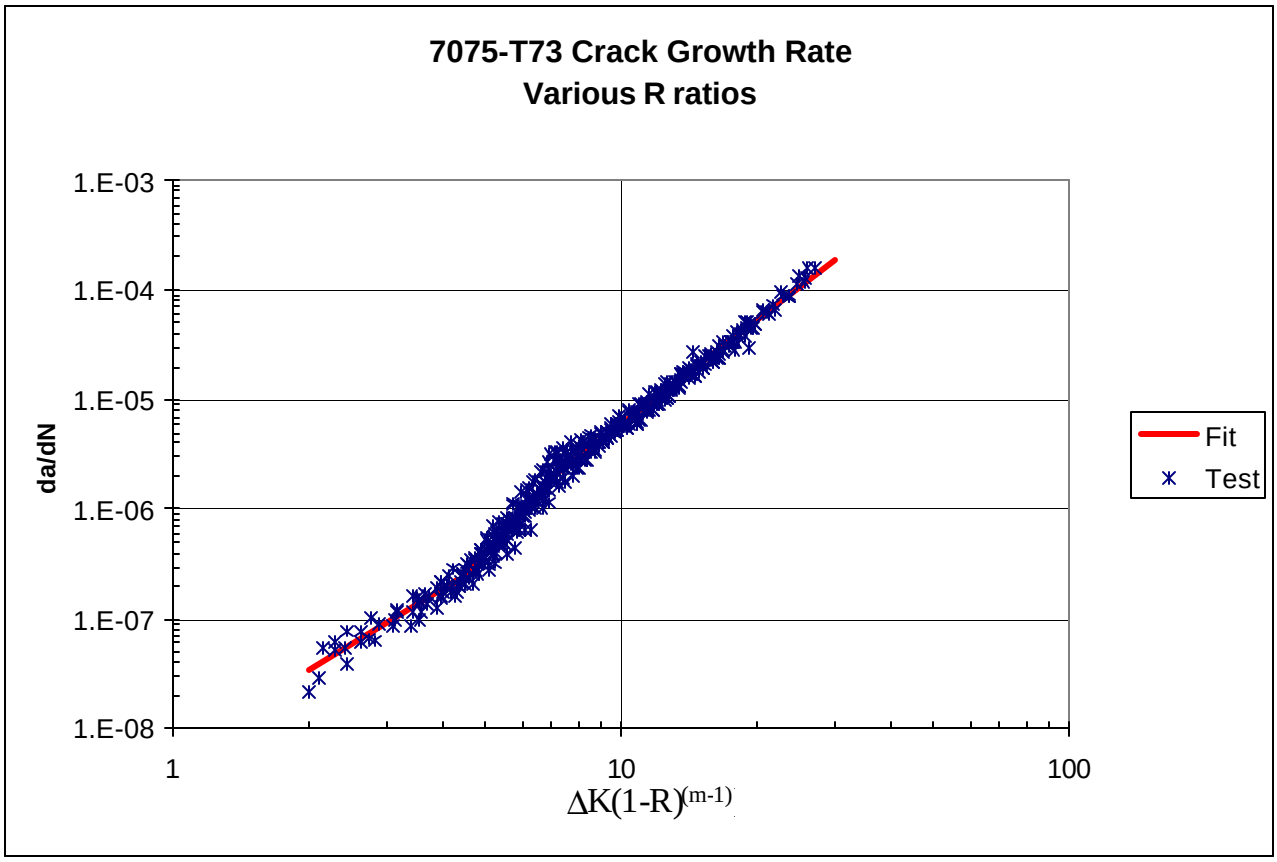

Figure 3-8 Crack Growth Rate Data Collapsed using the Walker Equation

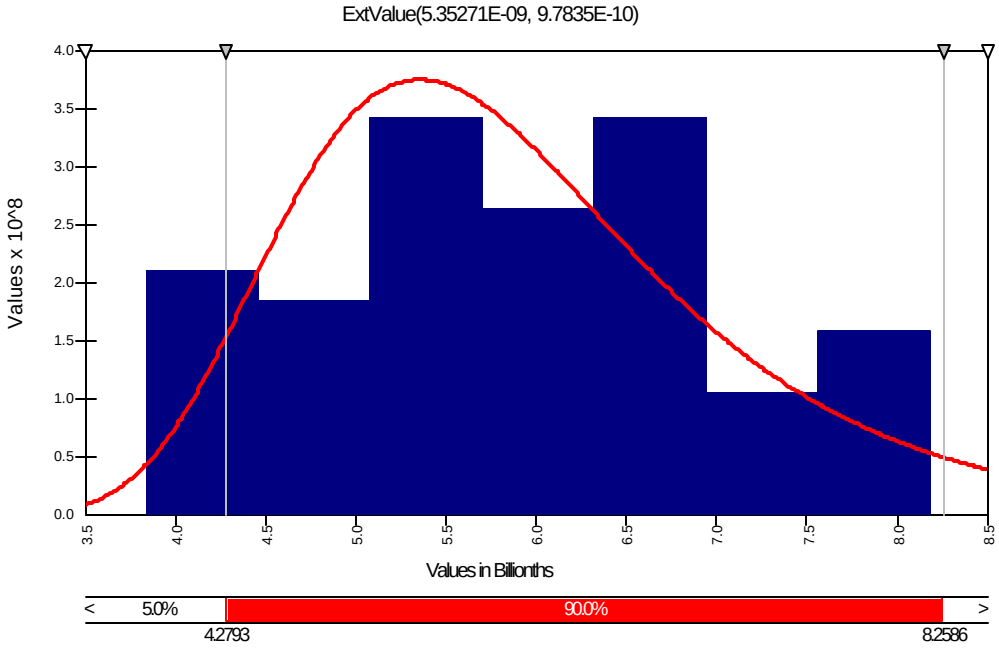

Figure 3-9 C1 Walker Constant Density Distribution

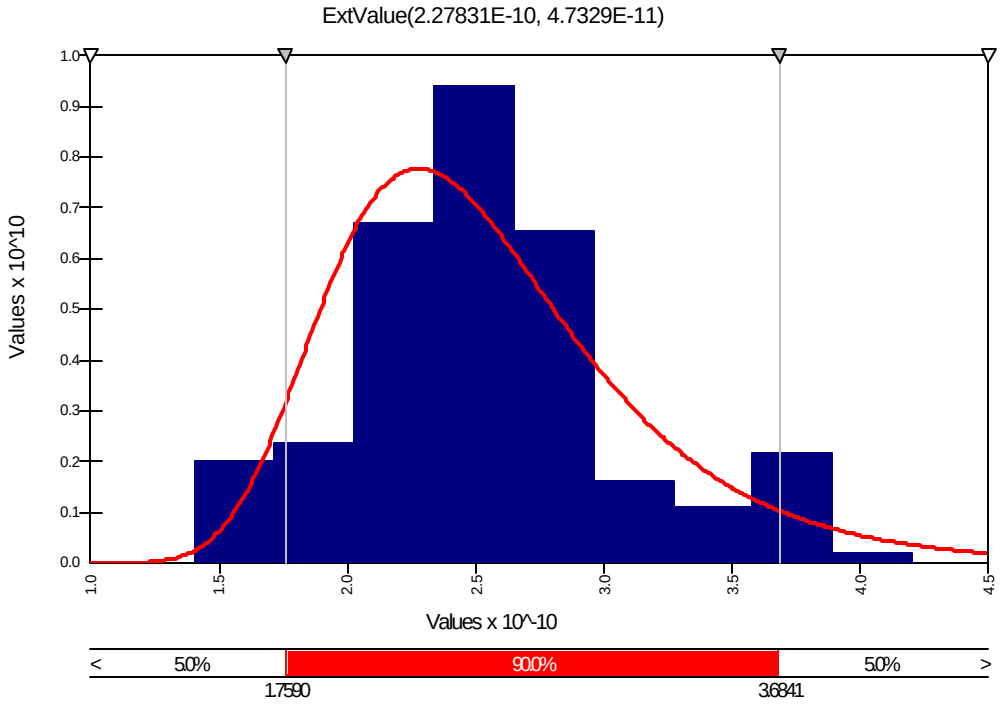

Figure 3-10 C2 Walker Constant Density Distribution

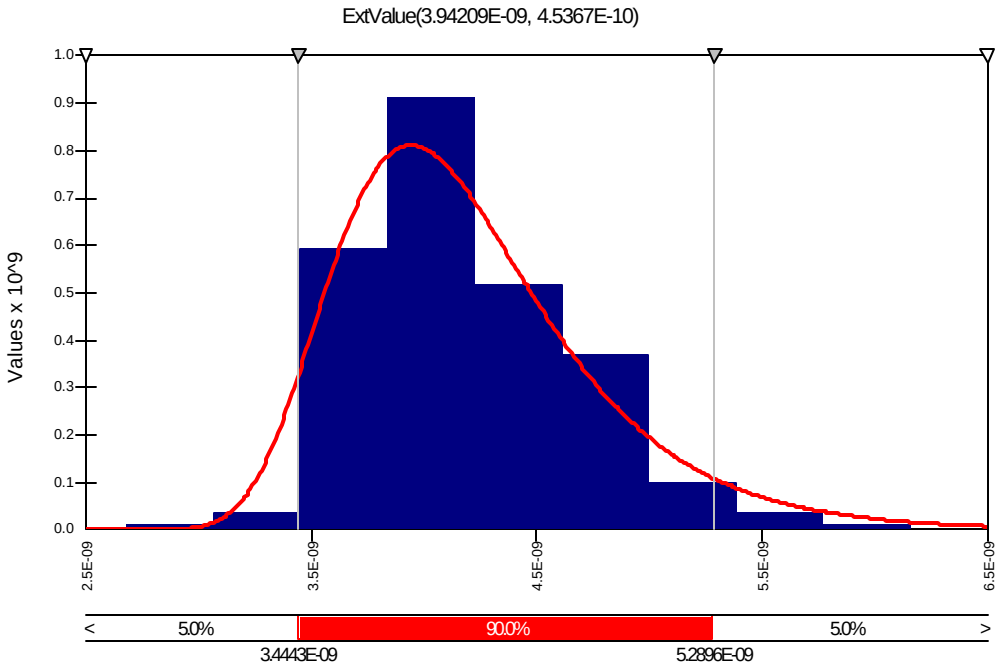

Figure 3-11 C3 Walker Constant Density Distribution

3.2 T-38 Specific Random Variables

The random variables specific to the T-38 are the fastener hole diameter, the fastener hole edge distance, the stress spectrum scale factor, and the retardation parameter. For the retardation parameter two different retardation models were used to investigate if the retardation model affected the results. In addition, retardation parameters were developed for the different aircraft usages.

The diameters of 46 holes in the lower wing skin were measured on a T-38 wing. The measurements were only accurate to 0.005 inches. Figure 3-12 shows a comparison to the measured distribution to the normal fit.

The fastener hole edge distance is based on 42 edge distance measurements made along the T-38 wing 15% spar on the left and right side of the wing. Figure 3-13 shows the edge distance comparison. As can be seen in this figure, the data is in two groups. This corresponds to measurements made on the left side or right side of the wing. This is expected, since the wing fastener holes are hand-drilled.

The stress spectrum scale factor in AFGROW was used as a random variable to try and represent uncertainties in the stress spectrum. Ideally, each stress level in the spectrum should be scaled independently of the other events. Unfortunately, with the current input data interface to AFGROW the entire spectrum is scaled by a single value. In order to develop the variation in this scale factor, data from a stress-to-load ratio project was used.

As part of a DTA update program for the T-38, SwRI used 1,189 flight measured strain gage reading to develop a stress to load ratio for the T-38 FCL A-15. The stress at this FCL is based on the wing bending moment at WS64.8. Based on a regression analysis of the strain gage data, the standard error for the stress component due to wing bending moment was 1.56%. Using the max spectrum stress from the IFF usage stress spectrum file of 21.71 ksi the standard deviation of the max spectrum stress is 0.34 ksi.

Retardation parameters were developed for two usages of this project, based on test results in [14]. In order to evaluate the effects of the retardation model on overall results, distributions were developed for the IFF usage for the generalized Willenborg retardation model and a closure retardation model. Five coupon test results were used to determine the IFF distributions. Figure 3-14 shows the IFF generalized Willenborg density distribution, and Figure 3-15 shows the IFF closure model density distribution. The Supplemental Undergraduate Pilot Training (SUPT) usage was only analyzed using the generalized Willenborg model. Figure 3-16 shows the SUPT generalized Willenborg density distribution for the three coupon tests. The retardation value distributions are based on a very small set of test data. Obviously more test data would be more rigorous.

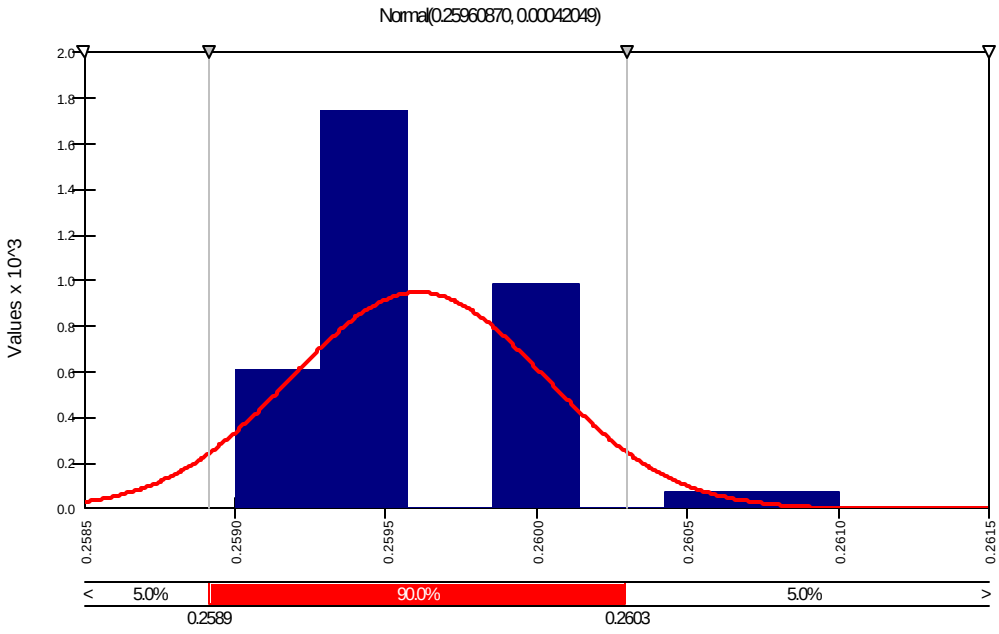

Figure 3-12 Fastener Hole Diameter Density Distribution

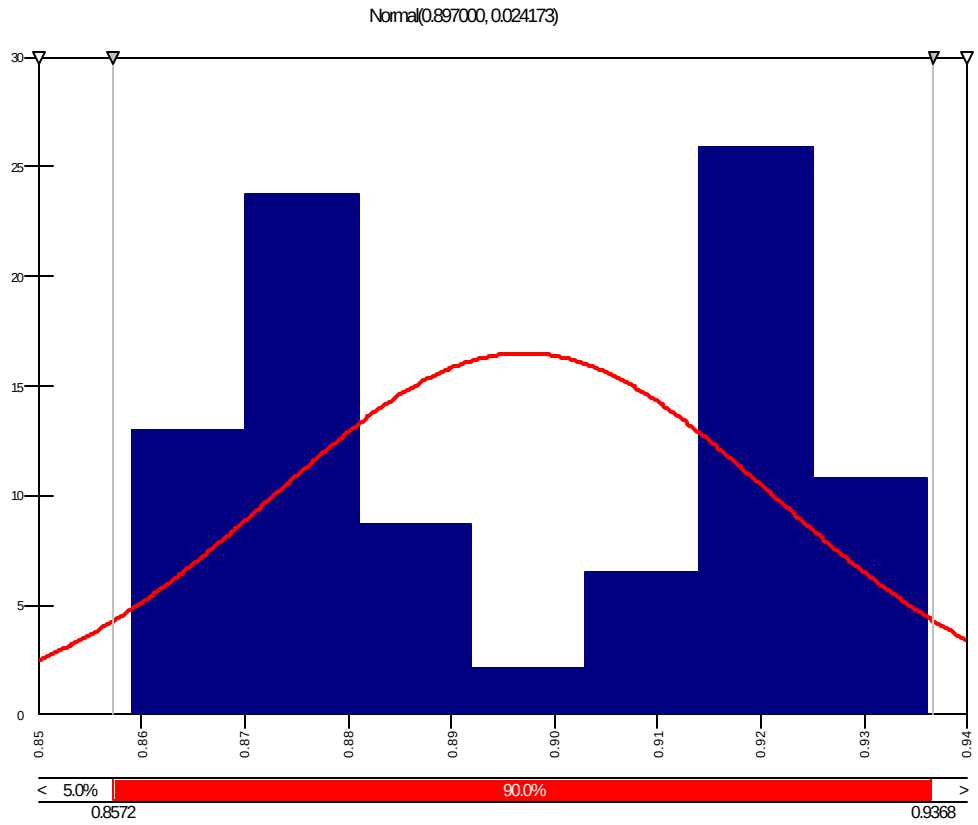

Figure 3-13 Edge Distance Density Distribution

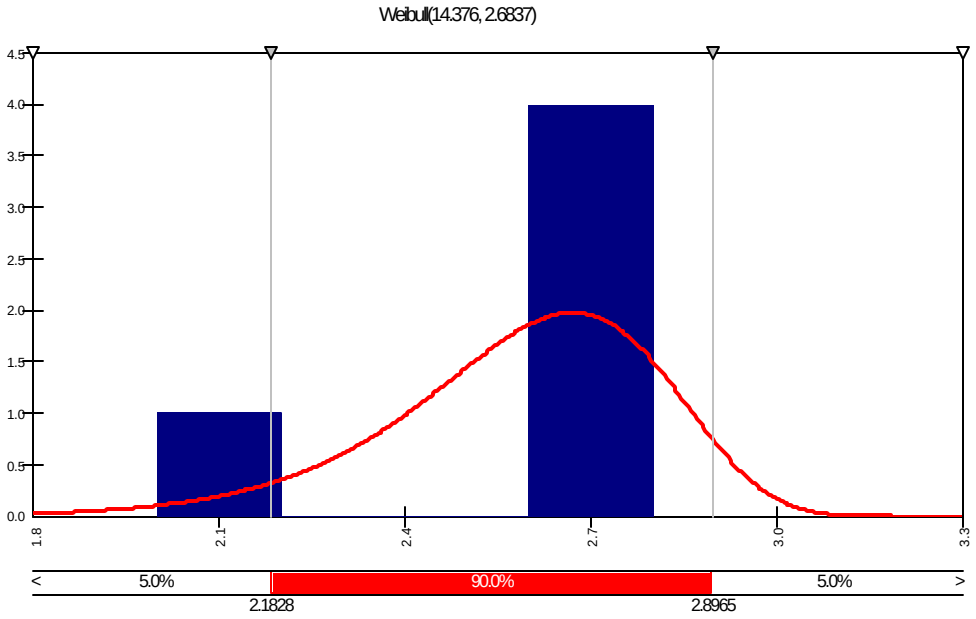

Figure 3-14 IFF Generalized Willenborg Retardation Model Density Distribution

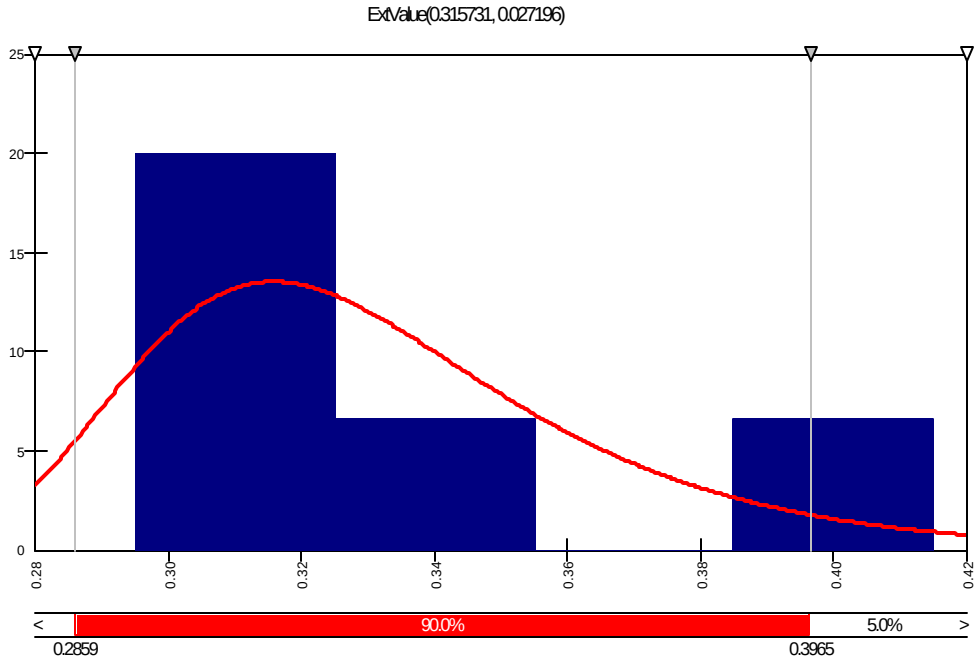

Figure 3-15 IFF Closure Retardation Model Density Distribution

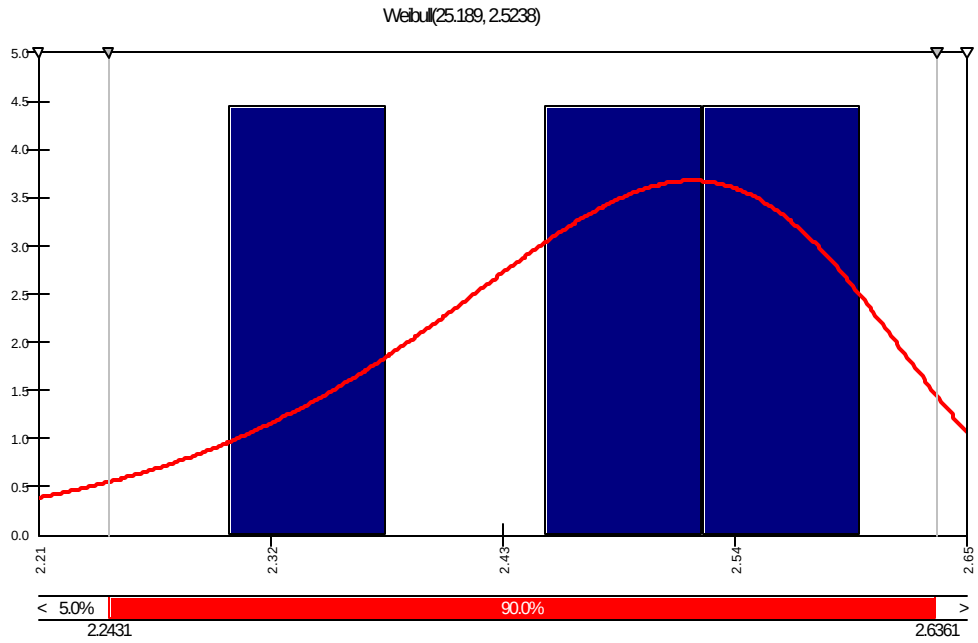

Figure 3-16 SUPT Generalized Willenborg Retardation Model Density Distribution

3.3 C-130 Specific Random Variables

The random variables specific to the C-130 are the fastener hole diameter, the fastener hole spacing, the fastener bearing stress ratio and spectrum stress scale factor. The C-130 fuselage stress spectra for the FCL analyzed is due solely to pressure cycles. The analysis was performed with a constant amplitude stress spectra so that there is no retardation. Teardown results are not available for the C-130 aircraft. SwRI has portions of C-141 available from limited fastener removal and measurements. Since both the C-130 and C-141 were manufactured by the same company in the same time frame, and have similar fuselage diameters and skin thicknesses, it was decided to use information from the C-141 for this project, and assume the C-130 data would be similar.

The diameters of 66 holes in the lower fuselage skin splice were measured on a C-141 fuselage. The measurements were only accurate to 0.005 inches. Figure 3-17 shows a comparison to the measured hole diameter distribution to the normal fit.

The C-130 fastener hole spacing is assumed to be the same as the C-141 spacing. The spacing is based on 30 C-141 measurements. Figure 3-18 shows the comparison between the measured spacing density distribution and the Weibull distribution.

From the C-130 DTA[2] the ratio of the bearing stress at the hole to the far field stress is 2.05. Data on how the bearing stress ratio varies is not available so we assumed the DTA bearing stress ratio was the mean and that the standard deviation was 10% of 2.05.

The C-130 FCL used for this study is loaded by pressure. The design limit pressure is 7.5 psi resulting in a skin hoop stress of 12.66 ksi. We assumed the standard deviation in the far field stress was 2.5% since we did not have any specific information on stress spectrum variation. The 2.5% is based on the measured variation in skin thickness. This resulted in a mean stress of 12.66 ksi and a standard deviation 0.3165 ksi.

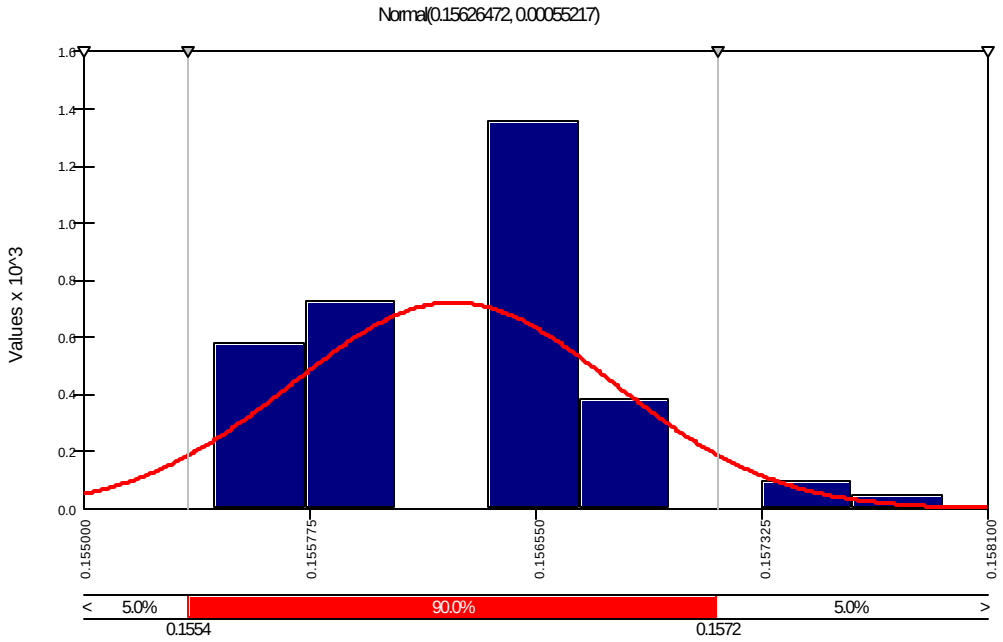

Figure 3-17 Fastener Hole Diameter Density Distribution

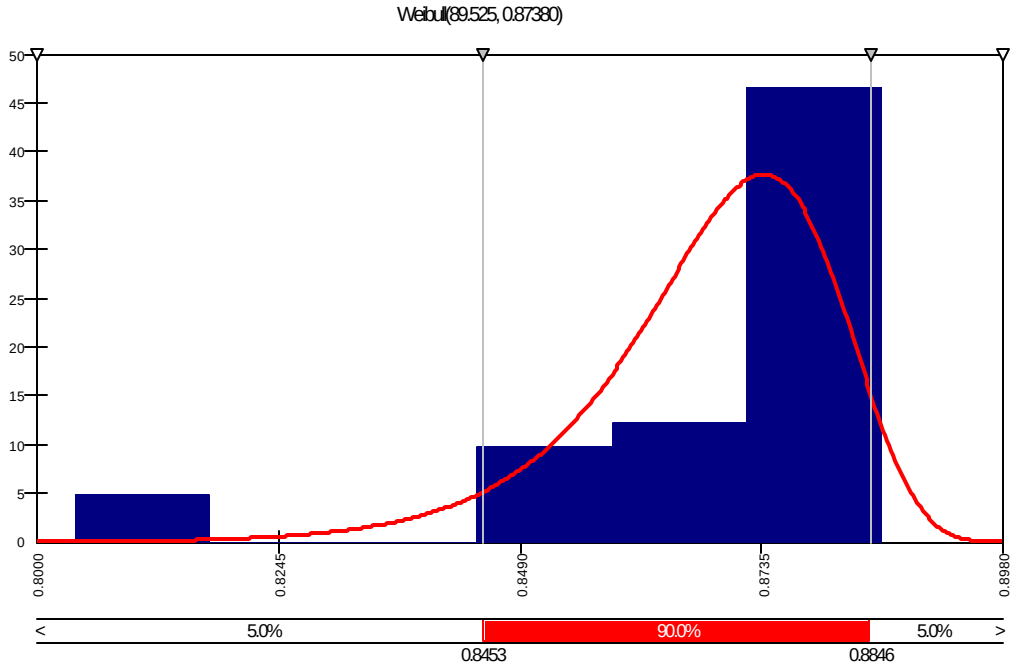

Figure 3-18 Fastener Spacing Density Distribution

4.0 T-38 PROBABILISTIC SENSITIVITY ANALYSIS

4.1 T-38 FCL A-15 Description

FCL A-15 is a countersunk fastener hole in the lower wing skin at WS 64.8 and the 15 percent spar (see Figure 4-1). It is stressed primarily by the wing bending moment. The nominal fastener hole diameter is 0.26 inches. The crack is assumed to grow from the base of the countersink to the free edge. The initial rogue flaw is approximated as a quarter-elliptical corner flaw.

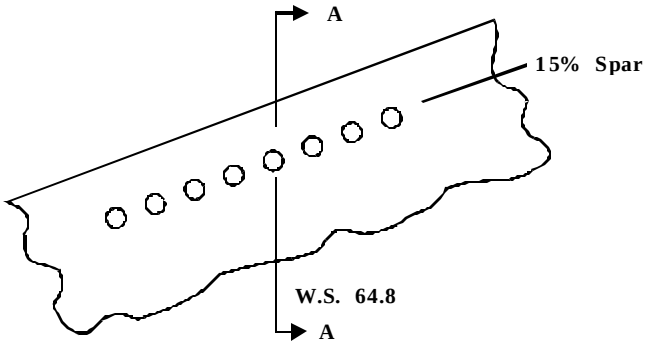

4.2 Spectrum Description

A large amount of actual aircraft usage data is available for use on this project. Three different spectra were chosen to give a large variation in the usage stress spectra. The NASA usage[15] was chosen as a very mild usage. The supplemental undergraduate pilot training (SUPT) usage[16] was chosen as an average usage. The introduction to fighter fundamentals (IFF) usage[17] was chosen as a sever usage spectra. Figure 4-2 is a normal load factor exceedance diagram comparison of the three usages. FCL A-15 stress spectra were developed for each usage. The maximum spectrum stress is 18.2 ksi, 22.1 ksi, and 21.7 ksi for the NASA, SUPT, and IFF usage respectively.

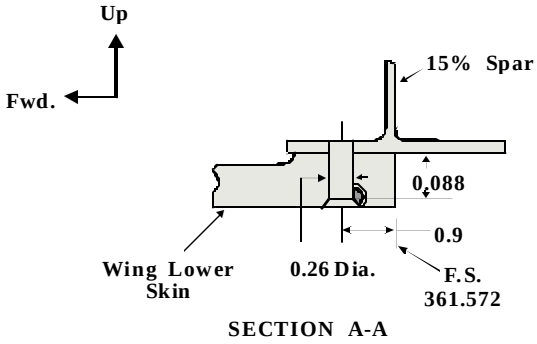

Figure 4-1 FCL A-15 Countersunk Fastener Hole at WS 64.8 and 15% Spar

4.3 Monte Carlo Simulation

Eight different Monte Carlo simulations were performed for T-38 FCL A-15 to evaluate changes in stress spectra, countersink correction factor idealization and retardation model effects. Each simulation consisted of 5,000 crack growth analysis runs with 12 or 13 random variables. In order to determine the effects of simplifying geometry assumptions a simulation was performed with and without the countersink correction factor on FCL A-15 for each usage. For the IFF and SUPT usages the simulation used the generalized Willenborg retardation random variables developed in Section 3.0. The NASA usage was assumed to be unretarded, since it is so mild. To investigate whether or not the retardation model chosen affected the overall results; the IFF simulations were repeated using the closure retardation model. The random variables, their mean, standard deviation and distribution type are given in Table 4-1.

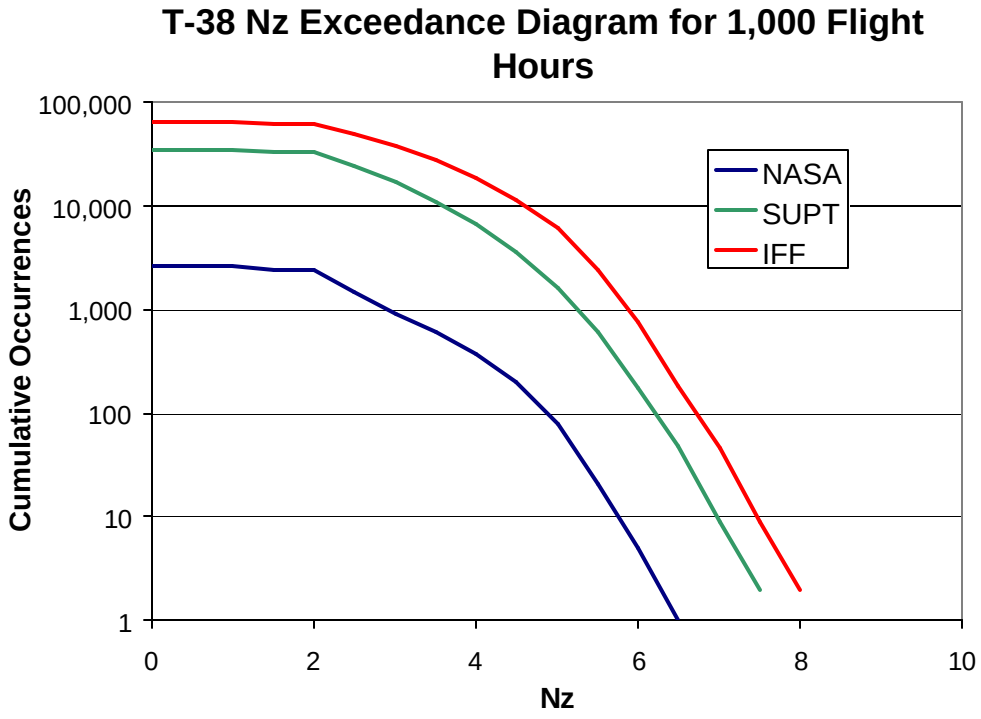

Figure 4-2 T-38 Normal Load Factor Exceedance Diagram

The mean and standard deviation results for the eight Monte Carlo Simulations are given in Table 4-2. As can be seen by examining this table, the choice of retardation model does not significantly affect the mean and standard deviation results. This table also demonstrates the importance of including the countersink correction factor in the crack growth analysis. There is about a 40% decrease in life when the countersink is modeled.

More importantly the random variable sensitivities for each analysis were determined at the 5% CDF level and the 50% CDF level. The relative importance of each random variable can be determined from sensitivity in terms of the change in probability with respect to a change in the mean or standard deviation of the random variables. The sensitivity definitions are: dprob/mean= $\frac{\partial P_f}{\partial m}$, and dprob/dstdev = $\frac{\partial P_f}{\partial s}$ these values are nondimensionalized as $\frac{\partial P_f}{\partial m} m$, and $\frac{\partial P_f}{\partial s} s$ and then normalized such that $\sum_{i=1}^{N} \left(\frac{dP_f}{dy} y \right)_i^2 = 1.0$ where y = mean or standard deviation. The values indicate the relative change in the probability of failure due to a change in random variable *i*.

Figure 4-3 and 4-4 show the normalized sensitivity results for FCL A-15 with the countersink modeled for the IFF usage for both retardation models. Figure 4-5 and 4-6 show the results without the countersink modeled. Both the sensitivity with respect to the

mean and standard deviation are shown. Figure 4-7 and 4-8 show the sensitivity results for the SUPT usage with and without the countersink. Figure 4-9 and 4-10 show the sensitivity results for the NASA usage.

Table 4-1 T-38 Random Variables

Variable	Mean	Standard Deviation	COV	Distribution
Initial Rogue Flaw Size (in.)	0.05	0.0045561	0.09	Weibull Offset 0.0446369
Crack Aspect Ratio	1.17713	0.36752	0.31	Extreme Value
Hole Diameter (in.)	0.2596087	0.0004205	0.00	Normal
Segment 1 Crack Growth Rate C1	5.92E-09	1.25E-09	0.21	Extreme Value
Segment 2 Crack Growth Rate C2	2.55E-10	6.07E-11	0.24	Extreme Value
Segment 3 Crack Growth Rate C3	4.20E-09	5.82E-10	0.14	Extreme Value
Hole Edge Distance (in.)	0.897	2.42E-02	0.03	Normal
Geometry Correction Factor (Beta)	1.009457	0.038067	0.04	Extreme Value
Yield Strength (ksi)	62.0247	3.6497	0.06	Normal
Plain Strain Fracture Toughness (ksi root in.)	33.6091	1.2526	0.04	Normal
Plain Stress Fracture Toughness (ksi root in.)	66.0389	2.9933	0.05	Normal
IFF Generalized Willenborg Retardation Parameter	2.588	0.22045	0.09	Weibull
IFF Closure Model Retardation Parameter	0.334	0.047749	0.14	Normal
IFF Stress Spectrum Scale Factor (ksi)	22.9	0.34	0.01	Normal
SUPT Generalized Willenborg Retardation Parameter	2.4697	0.12235	0.05	Weibull
SUPT Stress Spectrum Scale Factor (ksi)	22.9	0.34	0.01	Normal
NASA Stress Spectrum Scale Factor (ksi)	22.9	0.34	0.01	Normal

Table 4-2 T-38 Monte Carlo Results

Usage	Retardation Model	Countersink	Mean (Flight Hours)	Standard Deviation (Flight Hours)	COV
IFF	Willenborg	Yes	3310	793	0.24
IFF	Closure	Yes	3341	948	0.28
IFF	Willenborg	No	5504	2331	0.42
IFF	Closure	No	5840	2818	0.48
SUPT	Willenborg	Yes	15226	3509	0.23
SUPT	Willenborg	No	23687	9082	0.38
NASA	None	Yes	93870	21393	0.23
NASA	None	No	166219	81827	0.49

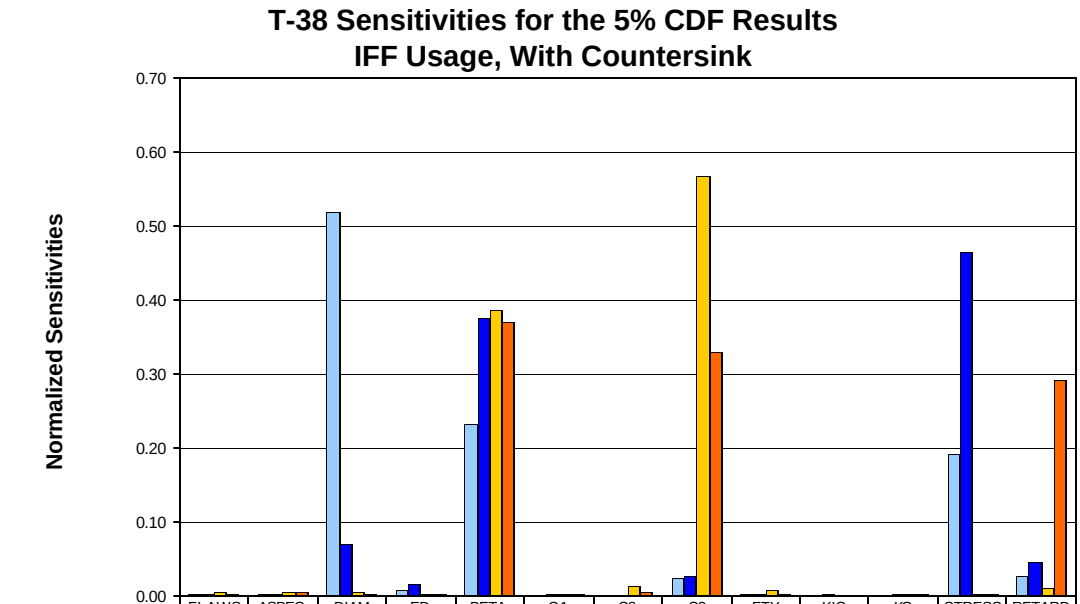

	FLAWS	ASPEC	DIAM	ED	BETA	C1	C2	C3	FTY	KIC	KC	STRESS	RETARD
Willenborg Mean	0.00	0.00	0.52	0.01	0.23	0.00	0.00	0.02	0.00	0.00	0.00	0.19	0.03
Closure Mean	0.00	0.00	0.07	0.02	0.38	0.00	0.00	0.03	0.00	0.00	0.00	0.46	0.05
Willenborg Stand. Dev.	0.00	0.00	0.00	0.00	0.39	0.00	0.01	0.57	0.01	0.00	0.00	0.00	0.01
Closure Stand. Dev.	0.00	0.00	0.00	0.00	0.37	0.00	0.01	0.33	0.00	0.00	0.00	0.00	0.29

Figure 4-3 5%CDF Sensitivities for the IFF Usage with a Countersink

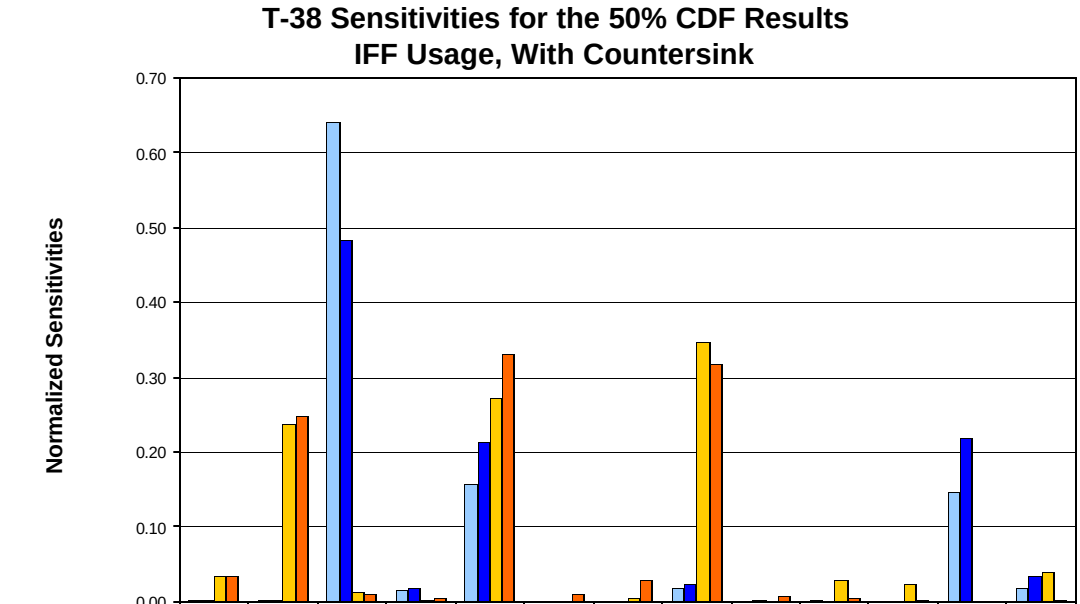

	FLAWS	ASPEC	DIAM	ED	BETA	C1	C2	C3	FTY	KIC	KC	STRESS	RETARD
Willenborg Mean	0.00	0.00	0.64	0.02	0.16	0.00	0.00	0.02	0.00	0.00	0.00	0.15	0.02
Closure Mean	0.00	0.00	0.48	0.02	0.21	0.00	0.00	0.02	0.00	0.00	0.00	0.22	0.04
Willenborg Stand. Dev.	0.04	0.24	0.01	0.00	0.27	0.00	0.01	0.35	0.00	0.03	0.02	0.00	0.04
Closure Stand. Dev.	0.03	0.25	0.01	0.00	0.33	0.01	0.03	0.32	0.01	0.01	0.00	0.00	0.00

Figure 4-4 50%CDF Sensitivities for the IFF Usage with a Countersink

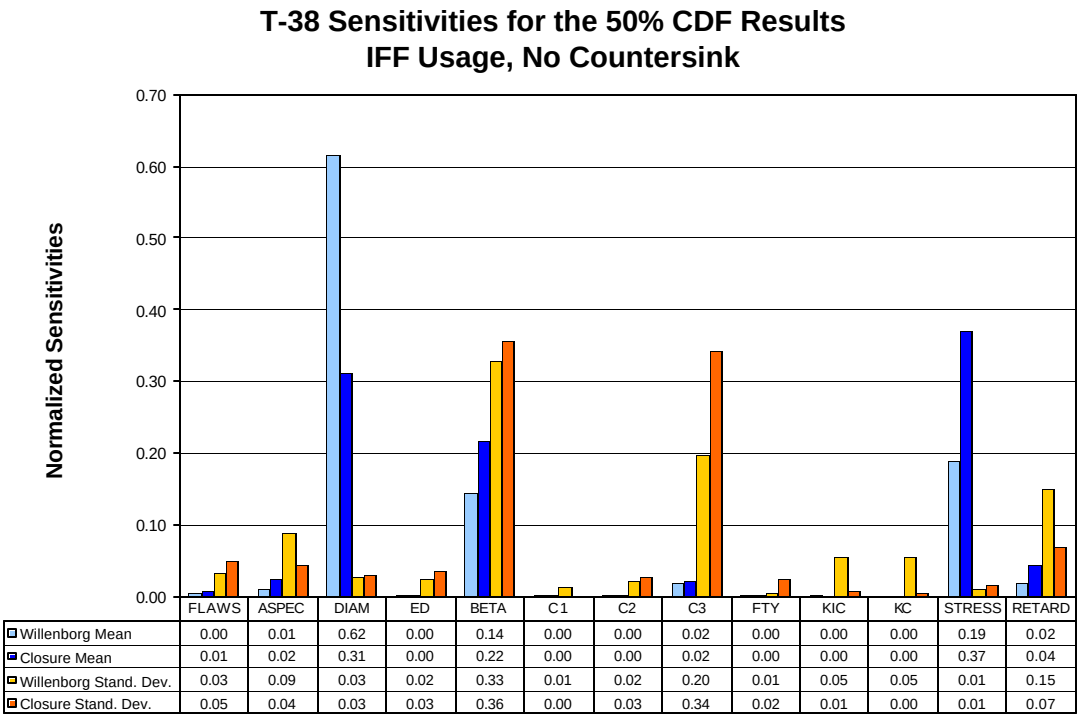

	FLAWS	ASPEC	DIAM	ED	BETA	C1	C2	C3	FTY	KIC	KC	STRESS	RETARD
Willenborg Mean	0.00	0.01	0.62	0.00	0.14	0.00	0.00	0.02	0.00	0.00	0.00	0.19	0.02
Closure Mean	0.01	0.02	0.31	0.00	0.22	0.00	0.00	0.02	0.00	0.00	0.00	0.37	0.04
Willenborg Stand. Dev.	0.03	0.09	0.03	0.02	0.33	0.01	0.02	0.20	0.01	0.05	0.05	0.01	0.15
Closure Stand. Dev.	0.05	0.04	0.03	0.03	0.36	0.00	0.03	0.34	0.02	0.01	0.00	0.01	0.07

Figure 4-5 50% CDF Sensitivities for the IFF Usage without a Countersink

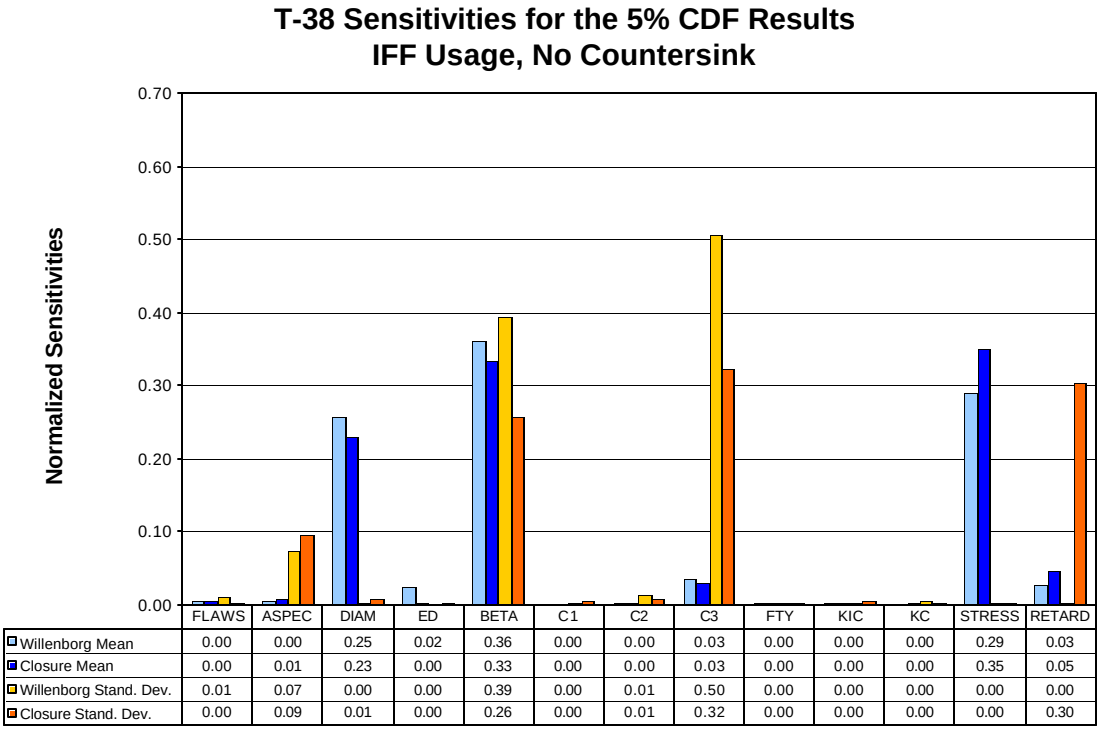

	FLAWS	ASPEC	DIAM	ED	BETA	C1	C2	C3	FTY	KIC	KC	STRESS	RETARD
Willenborg Mean	0.00	0.00	0.25	0.02	0.36	0.00	0.00	0.03	0.00	0.00	0.00	0.29	0.03
Closure Mean	0.00	0.01	0.23	0.00	0.33	0.00	0.00	0.03	0.00	0.00	0.00	0.35	0.05
Willenborg Stand. Dev.	0.01	0.07	0.00	0.00	0.39	0.00	0.01	0.50	0.00	0.00	0.00	0.00	0.00
Closure Stand. Dev.	0.00	0.09	0.01	0.00	0.26	0.00	0.01	0.32	0.00	0.00	0.00	0.00	0.30

Figure 4-6 5% CDF Sensitivities for the IFF Usage without a Countersink

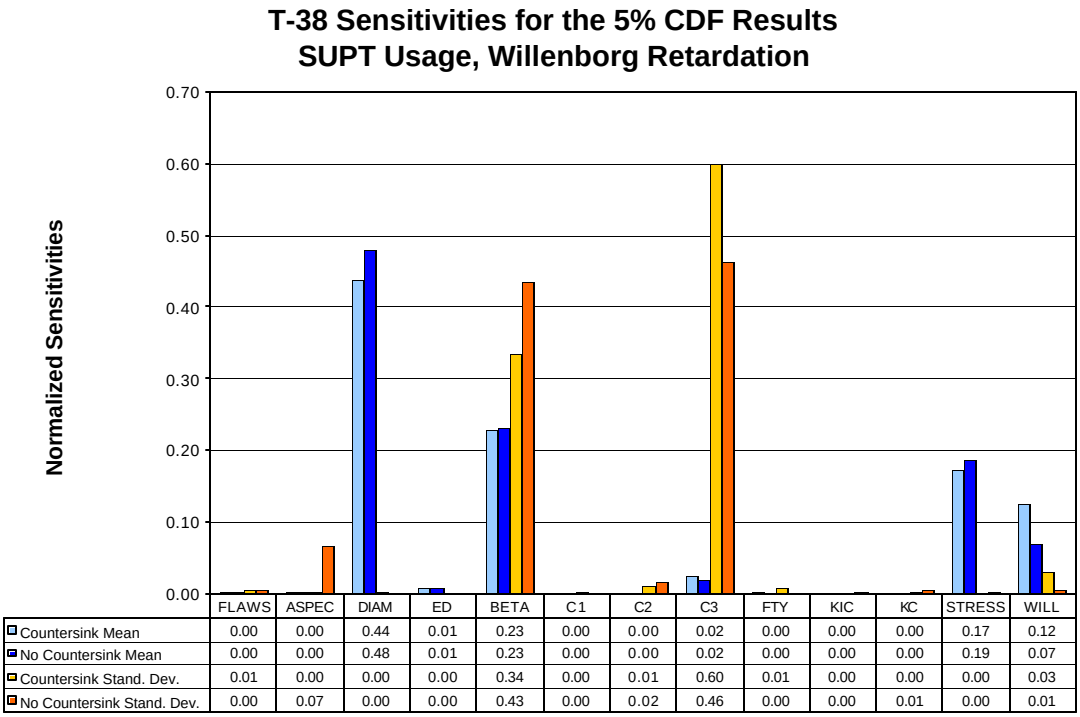

	FLAWS	ASPEC	DIAM	ED	BETA	C1	C2	C3	FTY	KIC	KC	STRESS	WILL
Countersink Mean	0.00	0.00	0.44	0.01	0.23	0.00	0.00	0.02	0.00	0.00	0.00	0.17	0.12
No Countersink Mean	0.00	0.00	0.48	0.01	0.23	0.00	0.00	0.02	0.00	0.00	0.00	0.19	0.07
Countersink Stand. Dev.	0.01	0.00	0.00	0.00	0.34	0.00	0.01	0.60	0.01	0.00	0.00	0.00	0.03
No Countersink Stand. Dev.	0.00	0.07	0.00	0.00	0.43	0.00	0.02	0.46	0.00	0.00	0.01	0.00	0.01

Figure 4-7 5% CDF Sensitivities for the SUPT Usage

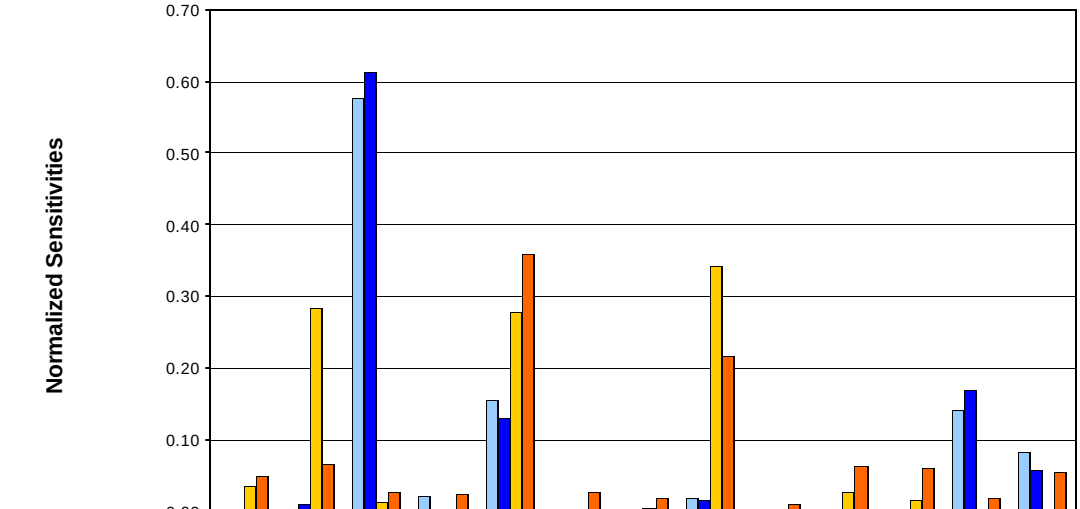

	FLAWS	ASPEC	DIAM	ED	BETA	C1	C2	C3	FTY	KIC	KC	STRESS	WILL
Countersink Mean	0.00	0.00	0.58	0.02	0.16	0.00	0.00	0.02	0.00	0.00	0.00	0.14	0.08
No Countersink Mean	0.00	0.01	0.61	0.00	0.13	0.00	0.00	0.01	0.00	0.00	0.00	0.17	0.06
Countersink Stand. Dev.	0.03	0.28	0.01	0.00	0.28	0.00	0.00	0.34	0.00	0.03	0.02	0.00	0.00
No Countersink Stand. Dev.	0.05	0.07	0.03	0.02	0.36	0.03	0.02	0.22	0.01	0.06	0.06	0.02	0.06

Figure 4-8 50% CDF Sensitivities for the SUPT Usage

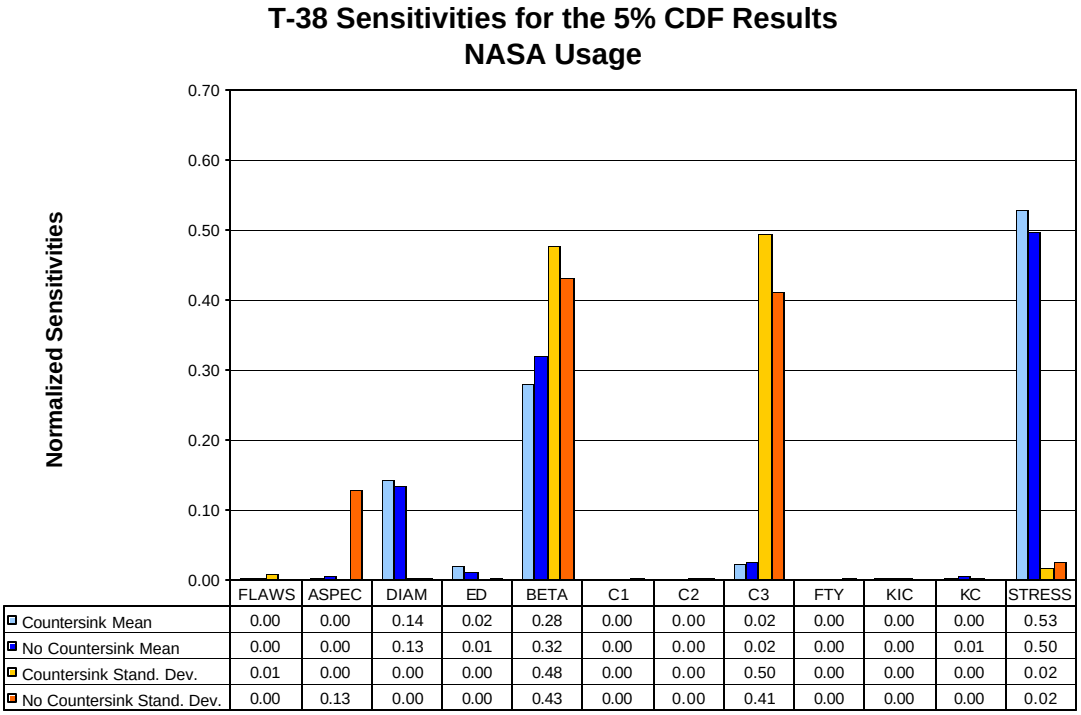

	FLAWS	ASPEC	DIAM	ED	BETA	C1	C2	C3	FTY	KIC	KC	STRESS
Countersink Mean	0.00	0.00	0.14	0.02	0.28	0.00	0.00	0.02	0.00	0.00	0.00	0.53
No Countersink Mean	0.00	0.00	0.13	0.01	0.32	0.00	0.00	0.02	0.00	0.00	0.01	0.50
Countersink Stand. Dev.	0.01	0.00	0.00	0.00	0.48	0.00	0.00	0.50	0.00	0.00	0.00	0.02
No Countersink Stand. Dev.	0.00	0.13	0.00	0.00	0.43	0.00	0.00	0.41	0.00	0.00	0.00	0.02

Figure 4-9 5% CDF Sensitivities for the NASA Usage

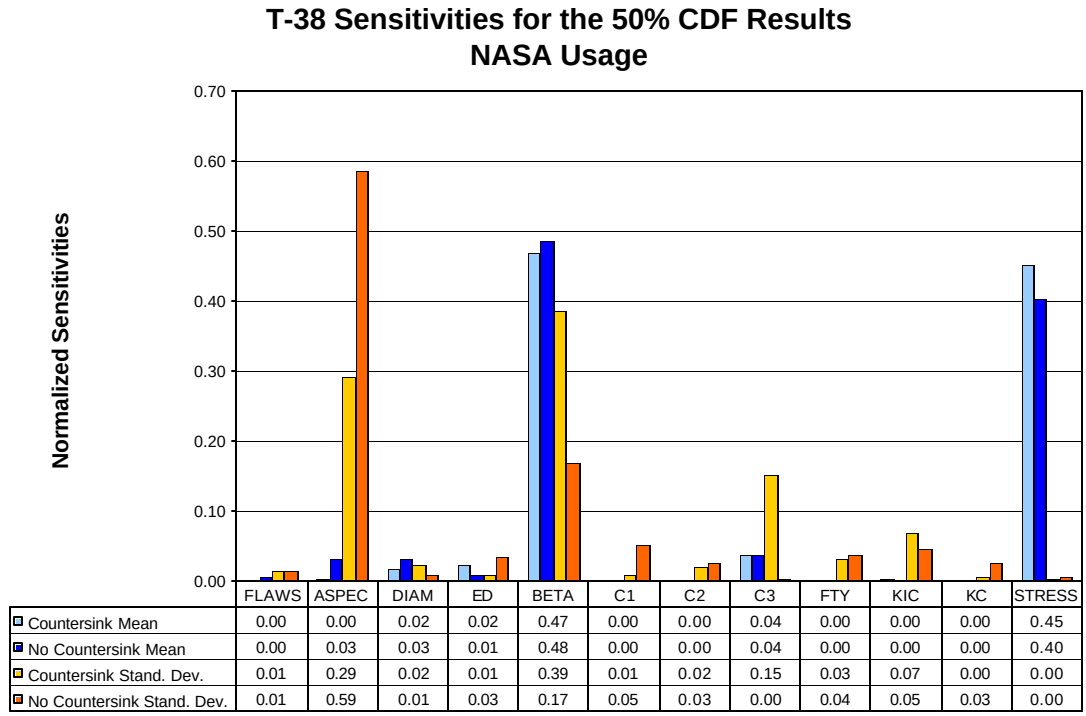

	FLAWS	ASPEC	DIAM	ED	BETA	C1	C2	C3	FTY	KIC	KC	STRESS
Countersink Mean	0.00	0.00	0.02	0.02	0.47	0.00	0.00	0.04	0.00	0.00	0.00	0.45
No Countersink Mean	0.00	0.03	0.03	0.01	0.48	0.00	0.00	0.04	0.00	0.00	0.00	0.40
Countersink Stand. Dev.	0.01	0.29	0.02	0.01	0.39	0.01	0.02	0.15	0.03	0.07	0.00	0.00
No Countersink Stand. Dev.	0.01	0.59	0.01	0.03	0.17	0.05	0.03	0.00	0.04	0.05	0.03	0.00

Figure 4-10 50% CDF Sensitivities for the NASA Usage

Careful review of figures 4-3 thru 4-10 reveals some interesting tendencies for T-38 FCL A-15. For all the parameters analyzed, the results are consistently sensitive to the fastener hole diameter, the geometry correction factor (beta), the crack growth rate at higher ΔKs (C3), and the stress spectrum scale factor. Of these variables, only the geometry correction factor is sensitive to variation in both the mean and standard deviation. Combining this fact with the observation that including the countersink geometry correction factor makes a large difference in life, an accurate geometry correction factor is critical.

The results are sensitive to the fastener hole diameter mean value but not its standard deviation. This would indicate that during the design process selecting the fastener hole diameter is critical but the typical manufacturing fastener hole diameter variation is acceptable from a damage tolerance perspective. The results are also sensitive to the mean value of the stress spectra scale factor. This is not surprising given that controlling the far field stress in a critical part of designing fatigue resistant parts. It is interesting that the results are not sensitive to the stress scale factor standard deviation. The results are sensitive to the standard deviation of the crack growth rate in the higher ΔK range. This would indicate that better process control in the material-manufacturing phase might help reduce scatter in damage tolerance life estimates.

For some cases the results are sensitive to the crack aspect ratio standard deviation but not the initial flaw size. This is likely due to the fact that a through crack is more severe than a corner crack. Thus, shorter cracks with large aspect ratios, which are nearly through cracks, can be more severe than longer cracks with small aspect ratios, which are still very much corner cracks.

The results are also occasionally sensitive to the retardation parameter. They appear to be most sensitive with respect for standard deviation for the closure model, 5% CDF results. This might indicate that the closure model is more sensitive to input parameters than the generalized Willenborg model for fast growing cracks. The simulation results and sensitivities are very similar for the two different retardation models. This indicates that the choice of retardation model is not a key analysis driver, as long as the retardation parameter is calibrated to test data.

It is interesting that the results are not sensitive to the material yield strength or either of the fracture toughness values. These values all affect the critical crack length. The fact that they are not critical indicates that for this FCL critical crack length is not important in calculating the total life of the part. Reviewing the DTA crack growth curve [1] for this FCL indicates that the crack is growing nearly vertically at the end of its life so that a large change in critical crack length does not translate into a large change in crack growth life.

5.0 C-130 PROBABILISTIC SENSITIVITY ANALYSIS

5.1 C-130 FCL CF-15 Description

FCL CF-15 is a countersunk fastener hole in the fuselage skin at the BL 61.6 skin splice between FS 679 and 737 (see Figure 5-1)[2]. It is stressed by fuselage pressurization. The nominal fastener hole diameter is 0.156 inches. The crack is assumed to grow from the base of the countersink to the next fastener hole. While the rogue flaw is growing the analysis assumes all the other fastener holes in line have an initial 0.005-inch manufacturing flaws that are all growing at the same time as the primary flaw. The crack continues growing from fastener hole to fastener hole until failure is reached. The initial rogue flaw is approximated as a through crack or a quarter-elliptical corner flaw depending weather or not the countersink is included. When the countersink is included in the analysis the skin is nearly in a knife-edge condition therefore the fracture mechanic model assumes the rogue flaw is a through crack. Figure 5-2 shows a typical crack growth analysis curve. The gaps in the curve represents the crack popping through to the next fasten hole.

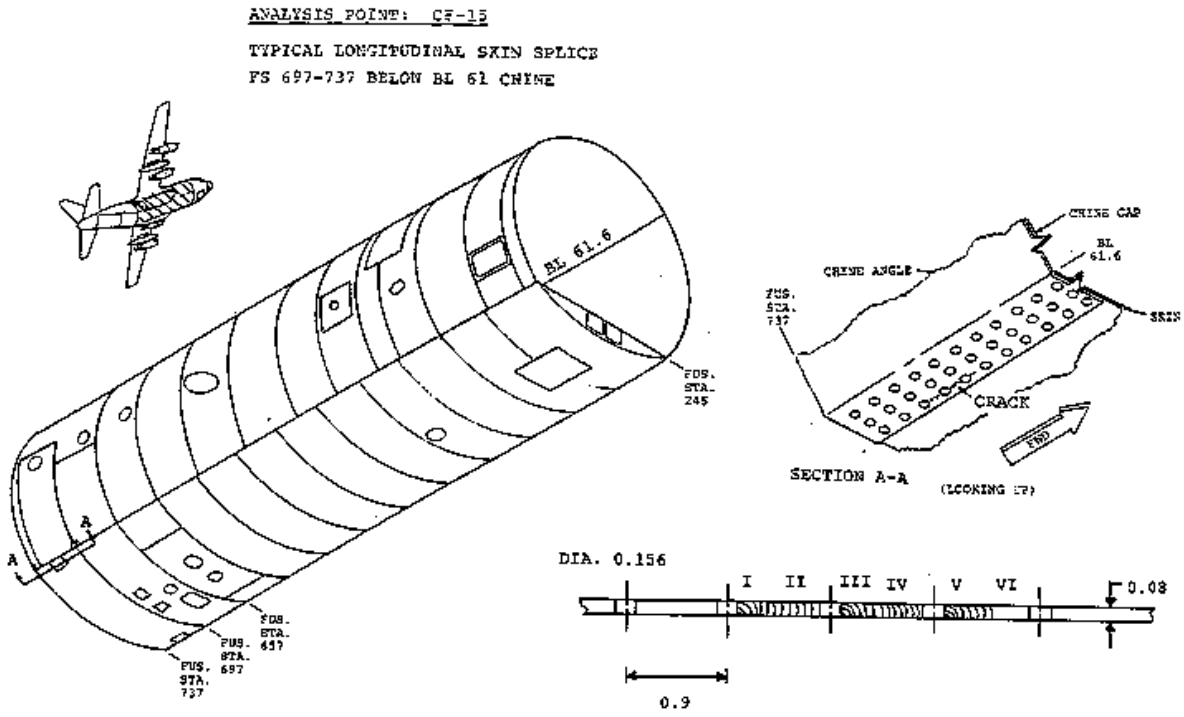

Figure 5-1 C-130 FCL CF-15

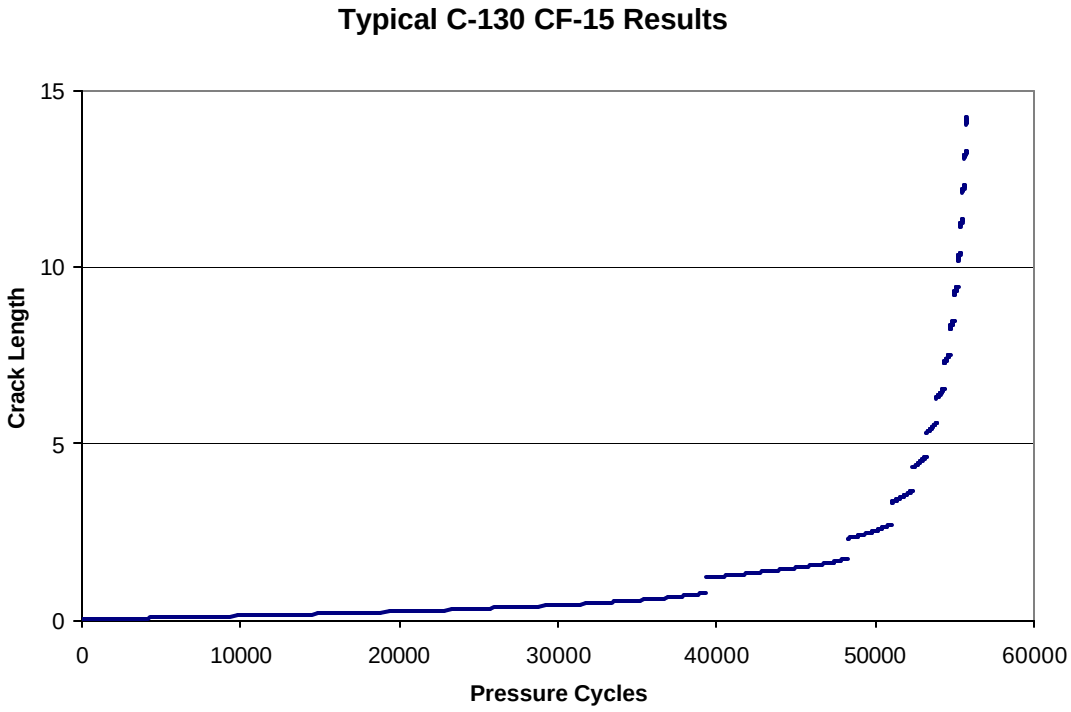

Figure 5-2 Typical C-130 Crack Growth Curve

5.2 Spectrum Description

The C-130 FCL CF-15 is assumed to be loaded by constant amplitude pressure cycles for this program. The skin stress is equal to 1,688 psi times the cabin pressure differential. The maximum pressure differential of 7.5 psi is reached at 18,500 feet altitude. This results in a limit design stress for this location of 12,660 psi. This is used as the constant amplitude stress level for the typical analysis. In order to investigate other constant amplitude loading conditions the stress was increased or decreased by a factor of 1.5 giving a maximum constant amplitude spectrum of 18,990 psi and a minimum spectrum of 8,440 psi.

5.3 Monte Carlo Simulation

Six different Monte Carlo simulations were performed for C-130 FCL CF-15 to evaluate changes in stress spectra and countersink correction factor. Each simulation consisted of 5,000 crack growth analysis runs. In order to determine the effects of simplifying geometry assumptions a simulation was performed with and without the countersink correction factor for FCL CF-15 for each stress level above. Since the spectrums are constant amplitude, all the simulations were performed unretarded. The random variables, their mean, standard deviation and equation are given in Table 5-1.

The mean and standard deviation results for the six Monte Carlo simulations are given in Table 5-2. This table demonstrates the importance of including the countersink

correction factor in the C-130 crack growth analysis. On average there is a 40% decrease in life when the countersink is modeled.

More importantly than determining the mean and standard deviation for the 6 NESSUS runs, the random variable sensitivities for each analysis were determined at the 5% CDF level and the 50% CDF level. Figures 5-3 and 5-4 show the normalized sensitivity results for FCL CF-15 with the countersink modeled for the 8.44 ksi constantan amplitude stress level is used with and without the countersink modeled. The 5% and 50% CDF levels respectively. Figure 5-5 and 5-6 show similar results for the 12.66 ksi constant amplitude loading. Figure 5-7 and 5-8 show the results for the 18.99 ksi constant amplitude loading. Both the sensitivity with respect to the mean and standard deviation are shown.

Table 5-1 C-130 Random Variables

Variable	Mean	Standard Deviation	COV	Distribution
Initial Rogue Flaw Size (in.)	0.05	0.0045561	0.09	Weibull Offset 0.0446369
Crack Aspect Ratio	1.17713	0.36752	0.31	Extreme Value
Hole Diameter (in.)	0.15626	0.0005522	0.004	Normal
Fastener Hole Spacing (in.)	0.86827	1.23E-02	0.01	Weibull
Geometry Correction Factor Variation (Beta)	1.009457	0.038067	0.04	Extreme Value
Bearing Stress Ratio	2.05	0.2	0.10	Normal
Crack Growth Rate Segment 1 (C1)	5.92E-09	1.25E-09	0.21	Extreme Value
Crack Growth Rate Segment 2 (C2)	2.55E-10	6.07E-11	0.24	Extreme Value
Crack Growth Rate Segment 3 (C3)	4.20E-09	5.82E-10	0.14	Extreme Value
Yield Strength (ksi)	62.0247	3.6497	0.06	Normal
Plain Strain Fracture Toughness (ksi root in.)	33.6091	1.2526	0.04	Normal
Plain Stress Fracture Toughness (ksi root in.)	66.0389	2.9933	0.05	Normal
Typical Pressurization Stress (ksi)	12.66	0.3165	0.03	Normal
Hi Pressurization Stress (ksi)	18.99	0.3165	0.02	Normal
Lo Pressurization Stress (ksi)	8.44	0.3165	0.04	Normal

Table 5-2 C-130 Monte Carlo Results

Constant Amplitude Stress Level	Countersink	Mean (Cycles to Failure)	Standard Deviation (Cycles)	COV
8.44 ksi	Yes	109810	23968	0.13
8.44 ksi	No	153668	45255	0.11
12.66 ksi	Yes	33985	4504	0.18
12.66 ksi	No	55585	5947	0.19
18.99 ksi	Yes	11855	2098	0.22
18.99 ksi	No	22406	4277	0.29

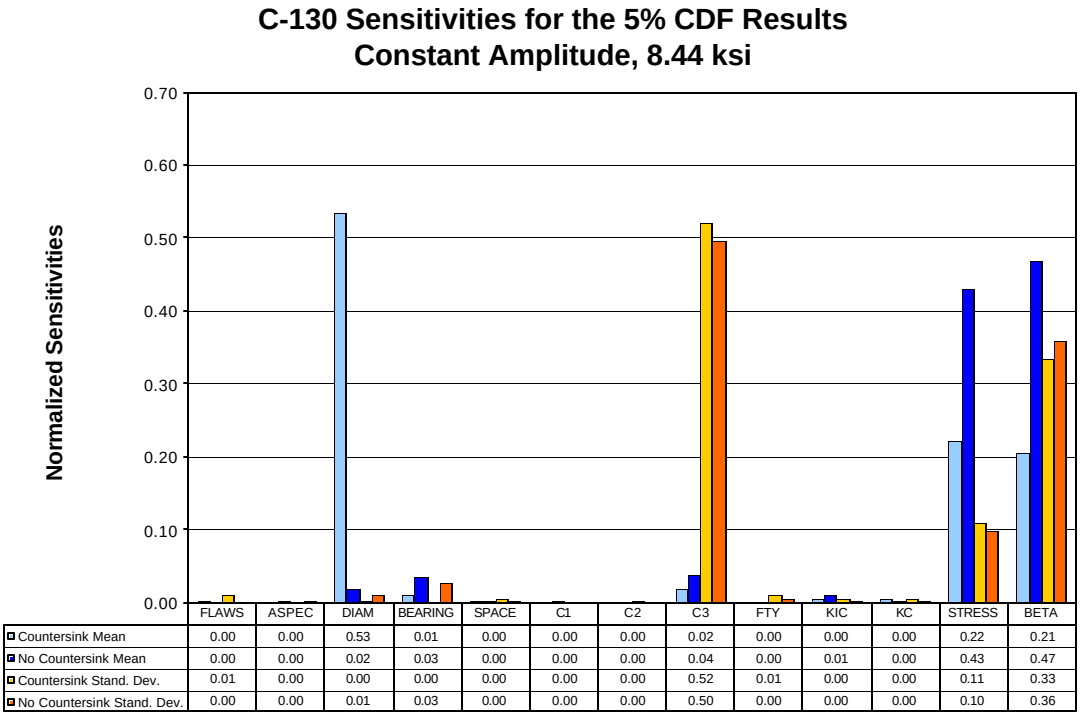

	FLAWS	ASPEC	DIAM	BEARING	SPACE	C1	C2	C3	FTY	KIC	KC	STRESS	BETA
Countersink Mean	0.00	0.00	0.53	0.01	0.00	0.00	0.00	0.02	0.00	0.00	0.00	0.22	0.21
No Countersink Mean	0.00	0.00	0.02	0.03	0.00	0.00	0.00	0.04	0.00	0.01	0.00	0.43	0.47
Countersink Stand. Dev.	0.01	0.00	0.00	0.00	0.00	0.00	0.00	0.52	0.01	0.00	0.00	0.11	0.33
No Countersink Stand. Dev.	0.00	0.00	0.01	0.03	0.00	0.00	0.00	0.50	0.00	0.00	0.00	0.10	0.36

Figure 5-3 8.44 ksi 5% CDF Sensitivity Results

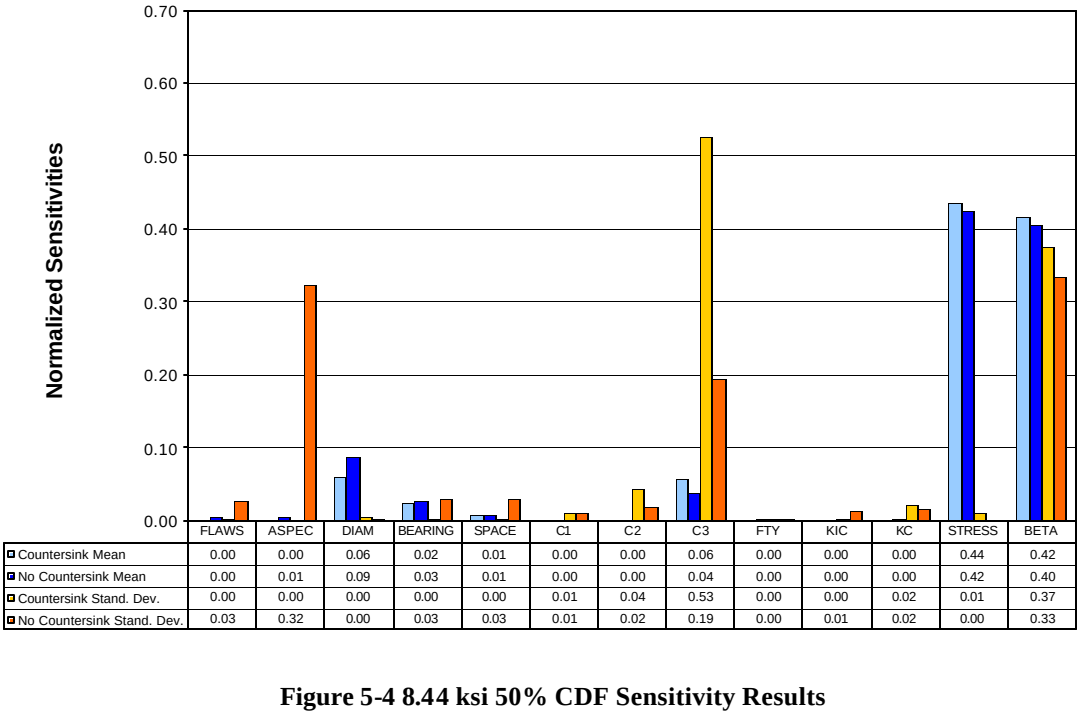

	FLAWS	ASPEC	DIAM	BEARING	SPACE	C1	C2	C3	FTY	KIC	KC	STRESS	BETA
Countersink Mean	0.00	0.00	0.06	0.02	0.01	0.00	0.00	0.06	0.00	0.00	0.00	0.44	0.42
No Countersink Mean	0.00	0.01	0.09	0.03	0.01	0.00	0.00	0.04	0.00	0.00	0.00	0.42	0.40
Countersink Stand. Dev.	0.00	0.00	0.00	0.00	0.00	0.01	0.04	0.53	0.00	0.00	0.02	0.01	0.37
No Countersink Stand. Dev.	0.03	0.32	0.00	0.03	0.03	0.01	0.02	0.19	0.00	0.01	0.02	0.00	0.33

Figure 5-4 8.44 ksi 50% CDF Sensitivity Results

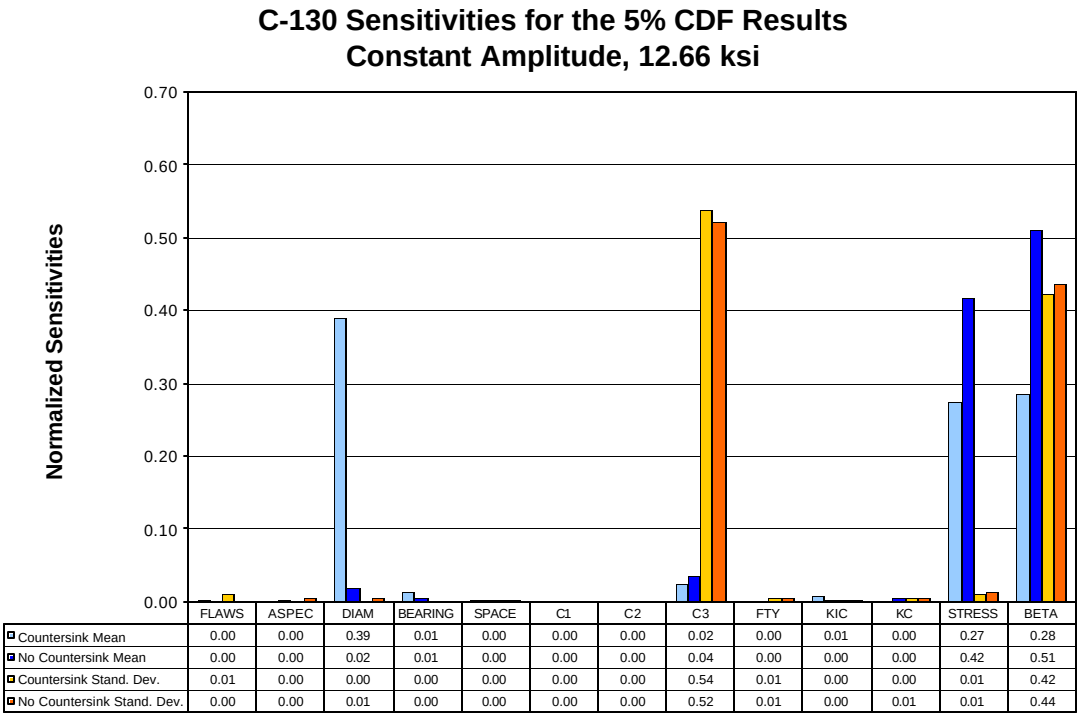

	FLAWS	ASPEC	DIAM	BEARING	SPACE	C1	C2	C3	FTY	KIC	KC	STRESS	BETA
Countersink Mean	0.00	0.00	0.39	0.01	0.00	0.00	0.00	0.02	0.00	0.01	0.00	0.27	0.28
No Countersink Mean	0.00	0.00	0.02	0.01	0.00	0.00	0.00	0.04	0.00	0.00	0.00	0.42	0.51
Countersink Stand. Dev.	0.01	0.00	0.00	0.00	0.00	0.00	0.00	0.54	0.01	0.00	0.00	0.01	0.42
No Countersink Stand. Dev.	0.00	0.00	0.01	0.00	0.00	0.00	0.00	0.52	0.01	0.00	0.01	0.01	0.44

Figure 5-5 12.66 44 ksi 5% CDF Sensitivity Results

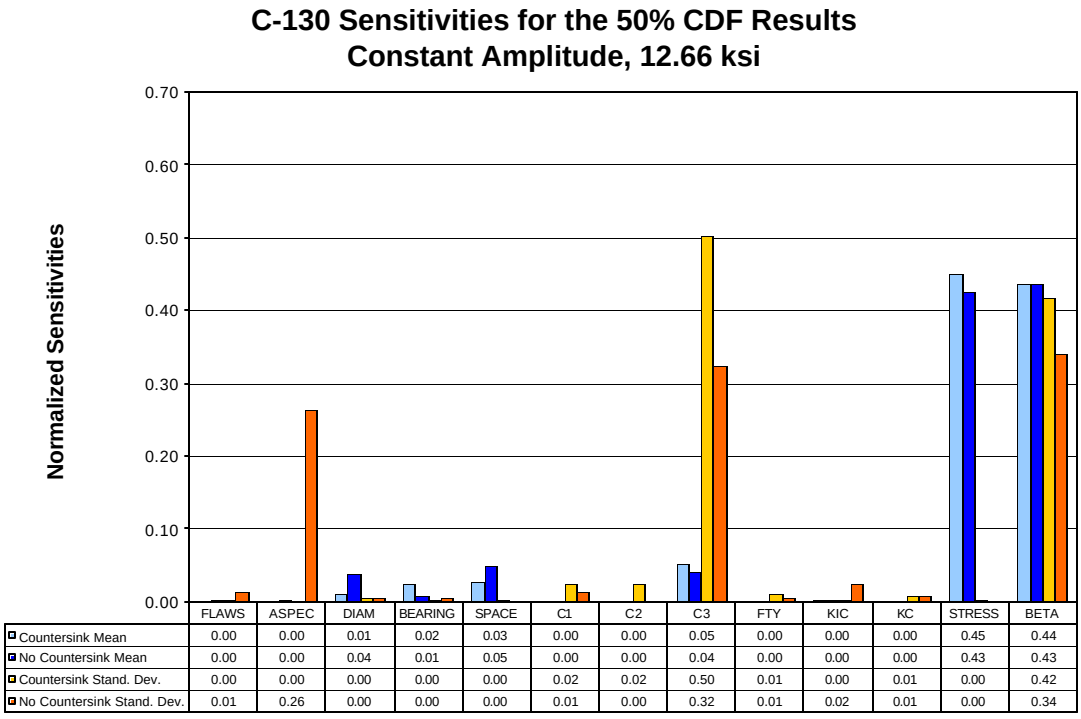

	FLAWS	ASPEC	DIAM	BEARING	SPACE	C1	C2	C3	FTY	KIC	KC	STRESS	BETA
Countersink Mean	0.00	0.00	0.01	0.02	0.03	0.00	0.00	0.05	0.00	0.00	0.00	0.45	0.44
No Countersink Mean	0.00	0.00	0.04	0.01	0.05	0.00	0.00	0.04	0.00	0.00	0.00	0.43	0.43
Countersink Stand. Dev.	0.00	0.00	0.00	0.00	0.00	0.02	0.02	0.50	0.01	0.00	0.01	0.00	0.42
No Countersink Stand. Dev.	0.01	0.26	0.00	0.00	0.00	0.01	0.00	0.32	0.01	0.02	0.01	0.00	0.34

Figure 5-6 12.66 44 ksi 50% CDF Sensitivity Results

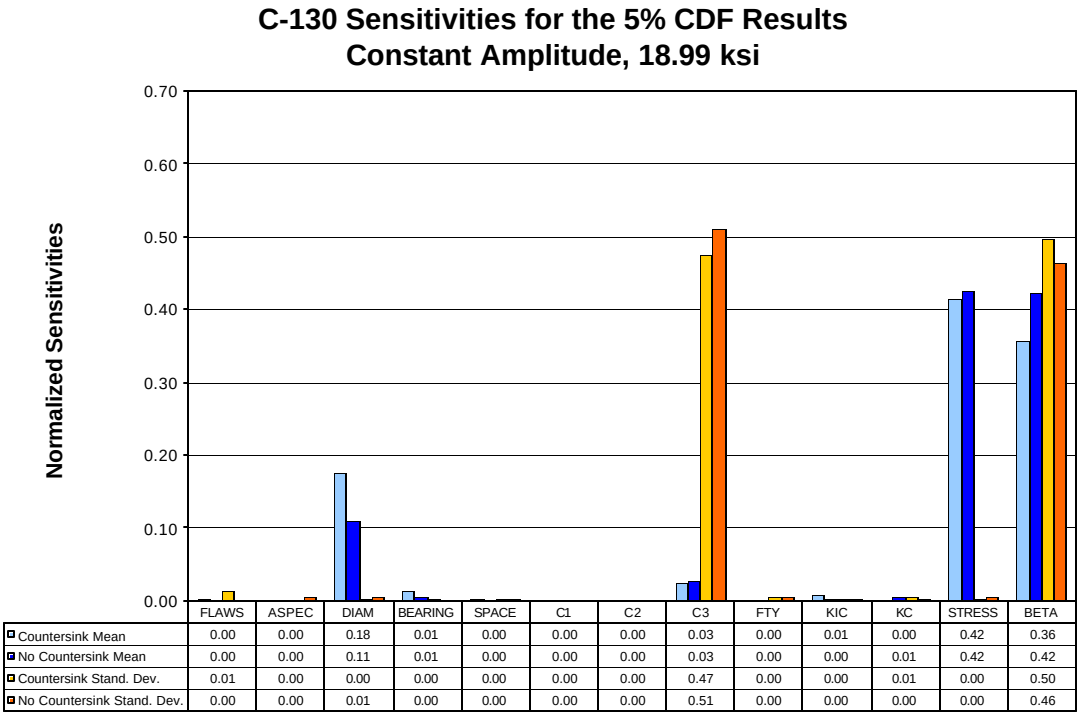

	FLAWS	ASPEC	DIAM	BEARING	SPACE	C1	C2	C3	FTY	KIC	KC	STRESS	BETA
Countersink Mean	0.00	0.00	0.18	0.01	0.00	0.00	0.00	0.03	0.00	0.01	0.00	0.42	0.36
No Countersink Mean	0.00	0.00	0.11	0.01	0.00	0.00	0.00	0.03	0.00	0.00	0.01	0.42	0.42
Countersink Stand. Dev.	0.01	0.00	0.00	0.00	0.00	0.00	0.00	0.47	0.00	0.00	0.01	0.00	0.50
No Countersink Stand. Dev.	0.00	0.00	0.01	0.00	0.00	0.00	0.00	0.51	0.00	0.00	0.00	0.00	0.46

Figure 5-7 18.99 ksi 5% CDF Sensitivity Results

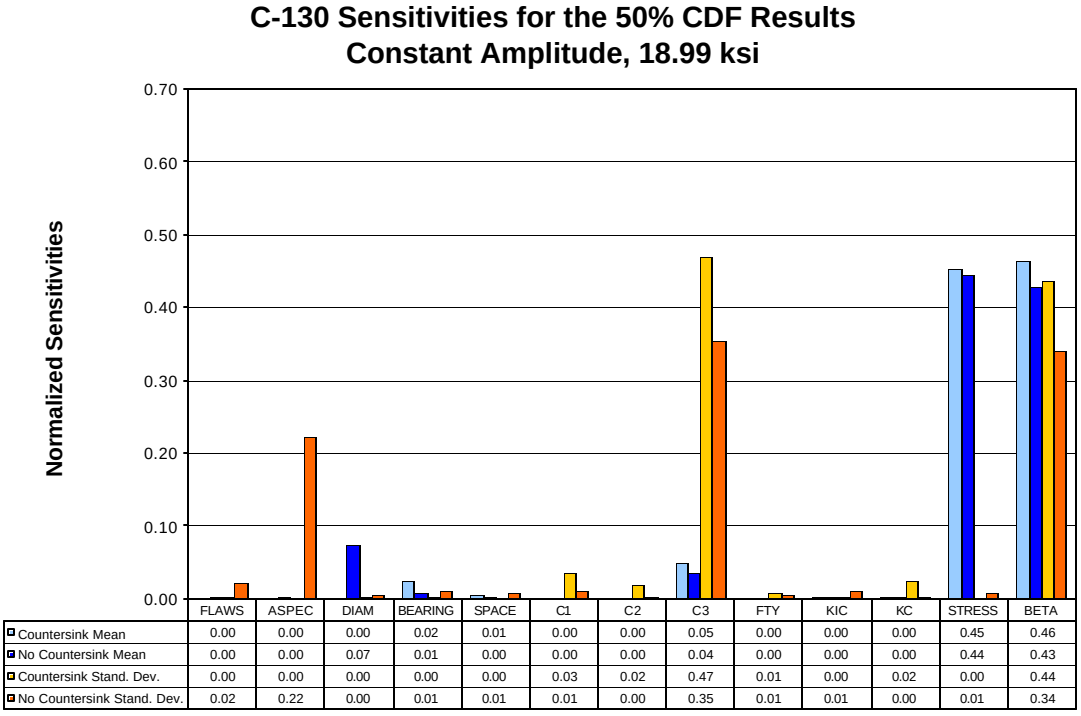

	FLAWS	ASPEC	DIAM	BEARING	SPACE	C1	C2	C3	FTY	KIC	KC	STRESS	BETA
Countersink Mean	0.00	0.00	0.00	0.02	0.01	0.00	0.00	0.05	0.00	0.00	0.00	0.45	0.46
No Countersink Mean	0.00	0.00	0.07	0.01	0.00	0.00	0.00	0.04	0.00	0.00	0.00	0.44	0.43
Countersink Stand. Dev.	0.00	0.00	0.00	0.00	0.00	0.03	0.02	0.47	0.01	0.00	0.02	0.00	0.44
No Countersink Stand. Dev.	0.02	0.22	0.00	0.01	0.01	0.01	0.00	0.35	0.01	0.01	0.00	0.01	0.34

Figure 5-8 18.99 ksi 50% CDF Sensitivity Results

Careful review of figures 5-3 thru 5-8 reveals some interesting tendencies for C-130 FCL CF-15. The results for the C-130 are very similar to the T-38 FCL. Of all the parameters analyzed the results are consistently sensitive to the geometry correction factor (beta), the crack growth rate at higher ΔKs (C3), and the variation in the stress spectrum scale factor. Of these variables only the geometry correction factor is sensitive to variation in both the mean and standard deviation. Combining this fact with the observation that whether or not the countersink is included in the geometry correction factor makes a large difference in life; thus, having an accurate geometry correction factor is critical.

The results are also sensitive to the mean value of the stress spectra scale factor. This is not surprising given that controlling the far field stress is a critical part of designing fatigue resistant parts. It is interesting that the results are not sensitive to the stress scale factor standard deviation. The results are sensitive to the standard deviation of the crack growth rate in the higher ΔK range. This would indicate that better process control in the material-manufacturing phase might help reduce scatter in damage tolerance life estimates.

For some analysis the results are sensitive to the crack aspect ratio standard deviation but not the initial flaw size. This is likely due to the fact that a through crack is more severe than a corner crack. Thus, shorter cracks with large aspect ratios, since these are nearly through cracks, can be more severe than longer cracks with small aspect ratios which are still very much corner cracks. Keep in mind that the countersunk fastener cases for the C-130 do not use the aspect ratio as a variable since it is in a near knife-edge condition. The 5% CDF results with countersunk are sensitive to the fastener hole diameter mean value but not its standard deviation. This is different from the T-38 FCL for which all the results were sensitive to the diameter mean value.

Again, it is interesting that the results are not sensitive to the material yield strength or either of the fracture toughnesses. Since these values all affect the critical crack length. The fact that they are not critical indicates that for this FCL critical crack length is not important in calculating the total life of the part. Reviewing the typical DTA crack growth curve in Figure 5-2 for this FCL indicates that the crack, again, is growing nearly vertically at the end of its life so that a large change in critical crack length does not translate into a large change in crack growth life.

The results are not sensitive to the bearing stress ratio or the fastener spacing. It is surprising that the results are not sensitive to the bearing stress ratio given that the results are so sensitive to changes in the overall geometry correction factor. It's possible that the results aren't sensitive to bearing due to the fact that the effects of bearing stress are very localized to the area near the fastener hole.

6.0 OBSERVATIONS, CONCLUSIONS AND RECOMMENDATIONS

This project performed probabilistic analysis on two FCLs. A T-38 lower wing fastener hole and a C-130 center fuselage skin splice fastener hole. A total of eight T-38 simulations and six C-130 simulations were performed. Each simulation included 5,000 crack growth runs. There were twelve or thirteen random variables analyzed for each simulation. Both FCLs were analyzed with and without countersink correction factors. The T-38 FCL was analyzed with two different retardation models for the IFF usage.

6.1 Observations

Both the T-38 and C-130 FCLs were sensitive to the geometry correction factor, the crack growth rate at higher ΔKs (C3) and stress spectrum scale factor for all the simulations. All the T-38 simulations and the C-130 5% CDF simulations were sensitive to the fastener hole diameter. In general the 50% CDF results were sensitive to the crack aspect ratio while the 5% CDF results were not. The choice of retardation model did not substantially effect the results. Modeling the countersink correction factor reduced the crack growth life by an average of 40%. Surprisingly the results were not sensitive to the initial flaw size. The results were also not sensitive to the yield strength, plain strain fracture toughness, plain stress fracture toughness, fastener hole edge distance, bearing stress ratio, fastener spacing, or the segment 1 and 2 crack growth rate data. The sensitivity results in generally are independent of the stress spectra analyzed, i.e. the IFF sensitivities are very similar to the SUPT sensitivities, which are very similar to the NASA sensitivities even though the mean flight hours to failure are very different.

6.2 Conclusions

The geometry correction factor (beta) is the only parameter that is sensitive to both the mean value and standard deviation for all the simulations. Including the effects of the countersink correction factor has a large effect on the overall simulation results. This indicates that properly modeling the stress intensity factors is critical for damage tolerance analysis and that oversimplification may be non-conservative.

The stress spectrum scale factor is sensitive to the mean value but not the standard deviation. This is an indication of the importance of having a good stress analysis that accurately predicts the state of stress at the FCL. It also indicates the importance of the stress levels in a component for determining the damage tolerance life. Due to funding limitations this program did not investigate the effects of variation in the usage spectrum. The fact that the results are sensitive to the stress scale factor would indicate the results might be sensitive to variations in the aircraft usage. This should be investigated in a future program.

The results are sensitive to the crack growth rate scatter in the higher ΔK range. This indicates that reducing the variation in crack growth rate may help reduce the scatter in damage tolerance test and analysis results.

The results for the T-38 and some of the C-130 results are sensitive to the hole diameter mean value. This is an indication in importance of selecting the correct fastener hole diameter in the design process.

The results are not sensitive to the faster spacing or edge distance (ED). This is a indication that relaxing the tolerance on hole placement may be possible as long as a minimum ED or fastener spacing is maintained. Relaxing the tolerance on fastener spacing could potentially speed up production.

The results are not sensitive to fracture toughness but are sensitive to the crack growth rate. This indicates that in the initial design process when materials are being selected; the crack growth rate may be a more important consideration than fracture toughness.

The T-38 IFF simulations investigated the effect of changing the retardation model. The simulation results are very similar for both retardation models. This indicates that choice of retardation model is not critical, as long as the retardation model is calibrated to actual spectrum tests. Development of a retardation model that does not require test calibration still has the potential to substantially reduce test costs.

6.3 Recommendation for Future Programs

Based on the results of this project the following recommendations are made for future funding. These recommendations are limited to the results of this project and may not be applicable to all FCLs or aircraft types. Future funding for DTA should be prioritized on:

Stress Intensity Factor Development
Stress Analysis and Stress Spectra Development
Crack Growth Rate Scatter Reduction
Implications to Structural Design

This project scope was limited due to funding limits. It is suggested that a follow-on program be funded to address these limitations. The follow-on program should address the effects of usage variation, effects of using initial flaw size distribution instead of a rogue flaw size, and the effects of performing inspections. A follow-on program should investigate different FCL geometries. The current project was limited to FCLs at fastener holes. This project could also investigate the applicability of advance sampling techniques, to reduce the simulation time. Would the sensitivities remain the same for lugs or surface cracks, or other geometries?

The probabilistic damage tolerance analysis techniques used in this program could easily be extended to the aircraft design process. This probabilistic DTA method will be an important part of certification by analysis of metallic structures. A follow-on project should be funded for the design of a metallic component using probabilistic DTA methods.

7.0 REFERENCES

1 SwRI Project Number 06-7278, “T-38 Durability and Damage Tolerance Analysis Update,” December 1998.

2 Lockheed-Georgia Co. Report No. LG81ER0152, “C-130 A/B/E/E*/H Durability and Damage Tolerance Assessment Summary Report,” December 1981.

3 Benjamin, J., and Cornell, C., Probability, Statistics, and Decisions for Civil Engineers, McGraw-Hill, 1970.

4 Ang, A.H.-S. and Tang, W., Probability Concepts in Engineering Planning and Design, Volumes I, John Wiley and Sons, New York, 1975.

5 Stephens, M., "Goodness of Fit with Special Reference to Tests for Exponentiality," Technical Report No. 262, Department of Statistics, Stanford University, Stanford, California, 1977.

6 Southwest Research Institute, "Probabilistic Structures Analysis Methods for Select Space Propulsion System Components (PSAM)," 1st-5th Annual Reports, NASA Contract NAS3-24389, 1985-1990.

7 Southwest Research Institute, "Probabilistic Structures Analysis Methods for Select Space Propulsion System Components (PSAM), Final Report, NASA Contract NAS3-24389, 1995.

8 Wu. Y.-T., "Computational Methods for Efficient Structural Reliability and Reliability Sensitivity Analysis," AIAA Journal, Vol. 32, pp. 1717-1723, 1994.

9 SwRI Project Number 06-5781, "Analytical Condition Inspection (ACI) of T-38 Wing Durability Test Article," December 1994.

10 SwRI Report “Evaluation of T-38 Wing Using Durability Test Results” Project No. 06-7257, April 1996.

11 SwRI Project Number 06-5906, “T-38 Coupon Spectrum Testing,” June 1995.

12 SwRI Project No. 06-4222 Report “F-5 FMS Durability and Damage Tolerance Update Revised Final DADTA Report - F-5E/F, Republic of Korea Air Force,” May 1996.

13 SwRI Project Number 7562/9, “T-38 -29 Wing Fatigue Critical Area Coupon Testing,” Final Report: Coupon and Additional Testing, September 1984.

14 SwRI Project Number 18-1334, "T-38 SUPT/IFF Coupon Analysis Results," March 2001.

15 SwRI Project Number 06-6927, “Usage and Preliminary Damage Tolerance Assessment Report for the National Aeronautics and Space Administration T-38A,” April 1996.

16 Letter to Mr. J. Dubke, SA-ALC/LADD, dated December 1, 1994, subject "T-38 AETC Flight Loads Data Recording for the SUPT Usage," SwRI Project Number 06-5898.

17 SwRI Project Number 06-6723, "Usage Assessment Report, AETC AT-38B Introduction to Fighter Fundamentals Pilot Training,” May 1997.